THE UNIVERSITY of EDINBURGH

Edinburgh Research Explorer

Speleothem evidence for MIS 5c and 5a sea level above modern level at Bermuda

Citation for published version:
Wainer, KAI, Rowe, MP, Thomas, AL, Mason, AJ, Williams, B, Tamisiea, ME, Williams, FH, Düsterhus, A & Henderson, GM 2017, 'Speleothem evidence for MIS 5c and 5a sea level above modern level at Bermuda', *Earth and Planetary Science Letters*, vol. 457, pp. 325-334. https://doi.org/10.1016/j.epsl.2016.10.005

Digital Object Identifier (DOI):
10.1016/j.epsl.2016.10.005

Link:
Link to publication record in Edinburgh Research Explorer

Document Version:
Peer reviewed version

Published In:
Earth and Planetary Science Letters

General rights
Copyright for the publications made accessible via the Edinburgh Research Explorer is retained by the author(s) and / or other copyright owners and it is a condition of accessing these publications that users recognise and abide by the legal requirements associated with these rights.

Take down policy
The University of Edinburgh has made every reasonable effort to ensure that Edinburgh Research Explorer content complies with UK legislation. If you believe that the public display of this file breaches copyright please contact openaccess@ed.ac.uk providing details, and we will remove access to the work immediately and investigate your claim.

OPEN ACCESS

Download date: 07. May. 2023

Highlights :

- U/Th constrained growth of Bermuda speleothems is analysed to reconstruct past sea level.

- Local relative sea level was at or above 1.5m during the MIS5e, c and a highstands.

- A double highstand peak above 1.5m is suggested during MIS5a.

- New constraints on the timing and maximum duration of MIS5 highstands are provided.

- These data can be used to constrain glacial isostatic adjustment models in the forebulge area.

*Manuscript
Click here to view linked References

Speleothem evidence for MIS 5c and 5a sea level above modern level at Bermuda

Karine A. I. Wainer[a], Mark P. Rowe[b], Alexander L. Thomas[c], Andrew J. Mason[a], Bruce Williams[d], Mark E. Tamisiea[e], Felicity H. Williams[f], André Düsterhus[g], Gideon M. Henderson[a]

[a] Department of Earth Sciences, Oxford University, South Parks Road, Oxford OX1 3AN, UK

[b] Department of Earth and Planetary Sciences, Birkbeck University of London, Malet Street, Bloomsbury, London WC1E 7HX, UK

[c] University of Edinburgh, West Mains Road, Edinburgh EH93JW, UK

[d] Bermuda Institute of Ocean Sciences, Bermuda

[e]National Oceanography Centre, Joseph Proudman Building, 6 Brownlow Street, Liverpool L3 5DA, UK

[f] National Oceanography Centre, University of Southampton, Waterfront Campus, European Way, Southampton SO14 3ZH, UK

[g] Institute of Oceanography, Centre for Earth System Research and Sustainability (CEN), University of Hamburg, Bundesstrasse 53, 20146 Hamburg, Germany

Corresponding author: K. Wainer, karinewainer@gmail.com

Other e-mail addresses:

M. Rowe: markprowe@gmail.com

A. Thomas: alex.thomas@ed.ac.uk

A. Mason: andrewm@earth.ox.ac.uk

B. Williams: Bruce.Williams@bios.edu

M. Tamisiea: metamisiea@gmail.com

F. Williams: Felicity.Williams@noc.soton.ac.uk

A. Düstherus: andre.duesterhus@uni-hamburg.de

G. Henderson: gideonh@earth.ox.ac.uk

Highlights :

- U/Th constrained growth of Bermuda speleothems is analysed to reconstruct past sea level.
- Local relative sea level was at or above 1.5m during MIS 5e, 5c and 5a highstands.
- A double highstand peak above 1.5m is suggested during MIS5a.
- New constraints on the timing and maximum duration of MIS5 highstands are provided.
- These data can be used to constrain glacial isostatic adjustment models in the forebulge area.

Keywords

Speleothem; sea level; Bermuda; isostasy; U-Th ages; forebulge.

Abstract

The history of sea level in regions impacted by glacio-isostasy provides constraints on past ice-sheet distribution and on the characteristics of deformation of the planet in response to loading. The Western North Atlantic-Caribbean region, and Bermuda in particular, is strongly affected by the glacial forebulge that forms as a result of the Laurentide ice-sheet present during glacial periods. The timing of growth of speleothems, at elevations close to sea level can provide records of minimum relative sea level (RSL). In this study we used U-Th dating to precisely date growth periods of speleothems from Bermuda which were found close to modern-day sea level. Results suggest that RSL at this location was above modern during

MIS5e, MIS5c and MIS5a. These data support controversial previous indications that Bermudian RSL was significantly higher than RSL at other locations during MIS5c and MIS5a. We confirm that it is possible to explain a wide range of MIS5c-a relative sea levels observed across the Western North Atlantic-Caribbean in glacial isostatic adjustment models, but only with a limited range of mantle deformation constants. This study demonstrates the particular power of Bermuda as a gauge for response of the forebulge to glacial loading, and demonstrates the potential for highstands at this location to be significantly higher than in other regions, helping to explain the high sea levels observed for Bermuda from earlier highstands.

1. Introduction

Bermuda is situated on the forebulge resulting from ice loading on North America during glacial periods (Fig. 1). Relative sea level (RSL) at Bermuda therefore has potential to provide information about the deformation parameters of the Earth, and/or about the distribution of past Laurentide and Greenland ice sheets. Conditions appear favourable for reconstruction of such RSL: tectonic activity is limited, and conditions are appropriate for both coral development and speleothem growth, allowing the use of two of the most robust sea-level archives that can be directly dated during this time interval. Nevertheless, the sea-level history of Bermuda remains uncertain (e.g. (Hearty, 2002; Rowe et al., 2014)), with the amplitude of highstands during the last interglacial complex (e.g. Marine Isotope Stage 5; MIS5) being particularly controversial.

It is now widely accepted that peak eustatic (i.e. global ocean mass equivalent) sea level of the Last Interglacial (e.g. MIS5e), was above modern (e.g. (Dutton and Lambeck, 2012; Dutton et al., 2015; Kopp et al., 2009)). The amplitude of subsequent smaller highstands during MIS 5c (~106-93 ka) and 5a (85-74 ka) is, however, generally more controversial. For MIS 5a, which is the better documented of the two, a large range of RSL has been reported around the globe, ranging from -30 m at the Huon Peninsula, Papua New Guinea (Lambeck and Chappell, 2001) to +5 m on the Atlantic coast of the US (Wehmiller et al., 2004). Within the Western North Atlantic-Caribbean (WNAC) region, the MIS 5a highstand has been reported at elevations ranging from -22 to +5 m (e.g. (Dodge et al., 1983; Dumas et al., 2006; Ludwig et al., 1996; Lundberg and Ford, 1994; Moseley et al., 2013; Muhs et al., 2002; Radtke and Schellmann, 2005; Richards et al., 1994; Toscano and Lundberg, 1999; Vacher and Hearty, 1989; Wehmiller et al., 2004). Such variability in WNAC RSL has been explained by glacio-isostatic adjustment (GIA) associated with the glacial forebulge (Potter and Lambeck, 2003). RSL in the North of the WNAC region is characterised particularly well by Bermuda, because it is a place where RSL records are available and is close to where GIA has the greater impact associated to the bulge (Fig.1). This makes accurate knowledge of RSL at Bermuda particularly useful, not principally for the information it provides about eustatic sea level, but for the constraints it provides on Earth deformation and regional ice sheet histories.

In this study, we present new MIS5 RSL data for Bermuda, based on high-resolution U-Th dating of speleothems. Speleothems are generally protected from weathering and many forms of erosion by their location, and can provide powerful archives of past sea-level change. Speleothems are also generally sampled when in growth position, and can only accrete when above sea level, thus periods of growth robustly indicate RSL below their site of formation

100 (Harmon et al., 1978; Moseley et al., 2013; Van Hengstum et al., 2015). Hiatuses in
101 speleothem growth indicate possible periods when sea level was above that level, but are less
102 robust indicators because other factors may lead to pauses in growth.

103

104 ## 2. Background

105 ### 2.1 MIS5 past sea-level reconstruction at Bermuda

106 The MIS5e highstand at Bermuda was higher than modern, as demonstrated by coral
107 occurrences up to +6 m, and a marine aragonite overgrowth on a stalactite from Crystal Cave
108 which developed during that period at +3 to +4 m (Harmon et al., 1981; Harmon et al., 1983;
109 Harmon et al., 1978). There are also a number of well-documented marine conglomerates up
110 to at least +9 m above modern sea level which, on the basis of U-series age data from
111 numerous coral fragments within them, can be attributed to MIS5e (Harmon et al., 1983;
112 Hearty and Kindler, 1995; Land et al., 1967; Meischner et al., 1995; Muhs et al., 2002). So
113 although the elevation of MIS5e RSL at Bermuda is not precisely established, it was clearly
114 above present-day level (Fig. 2).

115 On the contrary, the height of MIS 5c and 5a highstands at Bermuda is a contentious subject.
116 Evidence for the height of the MIS5c RSL highstand includes (Fig. 2):

117 • RSL above -6 m based on synchronous termination of growth of two speleothems; coral
118 fragments up to several meters above sea level dated ~100 ka (Harmon et al., 1978);
119 • RSL below -15 m based on a speleothem growing continuously from 110 ka to the
120 Holocene at -15 m, and on amino acid racemization ages on eolianites at ~105 (Harmon et
121 al., 1981);

- RSL above -15 m provided by rare corals in growth position dated from 105 to 97 ka (Vollbrecht, 1990);

Similar controversy exists for RSL during the MIS5a highstand (Fig. 2):

- RSL at 1-2 m based on a cluster of ages on coral fragments from 82 to 78 ka (Ludwig et al., 1996)
- RSL at a couple of meters above modern based on a cluster of ages on coral fragments from 84 to 78 ka (Muhs et al., 2002)
- RSL at 0-1 m based on amino-acid racemization data on land snails in a sub-aerial eolinite (Vacher and Hearty, 1989)

The strongest evidence suggesting RSL below modern for both MIS5c and 5a highstands is the continuous speleothem growth documented at -15 m from 110 ka to the Holocene (Harmon et al, 1981). The associated chronology for this sample is not completely robust due to the low precision and small number of α-counting U-Th ages. Potter and Lambeck (2003) suggested that the lack of a correction for initial Th might also explain the discrepancy between this RSL indicator and the rest of the literature, but the low ^{232}Th content of this sample argues against incorporation of significant initial ^{230}Th. It is perhaps more likely that the large quantity of material needed for dating by α-counting impedes establishment of a fine chronology to reveal potential hiatuses.

The strongest evidence for RSL above modern sea-level during MIS5c and 5a comes from the multiple coral fragment ages. The fact that these corals are not in life position, however, makes this constraint less robust. Ludwig et al. (1996) and Muhs et al. (2002) ruled out re-working on the basis of the exclusivity of the ages within the deposit, an idea supported recently by Rowe et al. (2014). Other authors have suggested that the coral fragments are found in storm deposits above sea level (e.g. Harmon et al., 1983), although this was

considered improbable given their position behind a wide reef-rimmed shallow lagoon (Vacher and Hearty, 1989).

The height of RSL at Bermuda during MIS5c and 5a therefore remains a controversial subject, reflected as well in various GIA models of the region which place it from above modern (Potter and Lambeck, 2003) to -20 m (Raymo and Mitrovica, 2012). Lack of robust observational constraint on the height of Bermuda RSL prevents the reliable use of this location to refine such GIA models and fulfil the potential of Bermuda as a recorder of the behaviour of the forebulge during ice-sheet loading and unloading. New evidence for RSL height during these periods are required to achieve that potential.

2.2 Multiple highstands during MIS5a in the Northern Hemisphere

In the WNAC, some records like terrace-coral records from Haiti and Barbados proposed multiple highstands during MIS5e, 5c and 5a (e.g. Radtke et al. 2005, Dumas et al. 2006). Regarding MIS5a, a consensus seems to identify a double highstand with an early short lived highstand centred on 84 ka and a second one centred on 77 ka (Dumas et al., 2006; Potter et al., 2004; Potter and Lambeck, 2003). A similar double peak feature is observed in the percentage of Quercus pollen in the nearby marine core, ODP1059, attesting that climate in the SE United States experienced two distinct warmer episodes coeval to these highstand peaks (Heusser and Oppo, 2003). Outside the WNAC area during MIS5a, the Red Sea record yields multiple sea-level oscillations of decreasing height (Rohling et al., 2009) and a submerged speleothems study in the Adriatic Sea, documents two highstand peaks, from 87 to 82 ka and from 77 to 64 ka (Surić et al., 2009). Although some of these locations are tectonically unstable, this suggests that high frequency fluctuations of sea level during MIS5a

may have been a global feature. Evidence from more tectonically stable locations, such as Bermuda, would help to confirm or refute this suggestion.

3. Site

Bermuda (32.3°N, 64.8°W) is a volcanic seamount with a continuous carbonate cap located in the central-western Atlantic (Fig. 1). It consists of a group of islands which were formed principally as a result of short-distance wind transportation, accumulation and lithification of carbonate grains and debris produced on the marine platform during sea-level cycles. Numerous caves have developed in the oldest formations of these carbonate islands. Climate in Bermuda, largely influenced by its location in the path of the Westerlies, is subtropical and humid with mean annual air temperature ~ 21°C and average rainfall ~1500 mm/year.

For this study, we sampled five caves. Key samples come from Wilkinson Quarry Cave, located on the north shore of the main island of Bermuda (32°21'N, 64°42'W, fig. S4). Access to the cave is no longer possible due to the danger of collapse caused by extensive work in the overlying quarry. This danger prevents contemporary monitoring of environmental parameters in this particular cave, but neighbouring Squeeze Cave, Admiral's Cave, Crystal Cave and Walsingham Cave, are within 1 km and provide information about the characteristics of karstic sites in the area. The location of all caves is shown on Fig. S4 in the supplemental material.

3. Water level monitoring

Wilkinson Quarry, Squeeze, Admiral's, Crystal and Walsingham caves are well connected to the ocean largely through secondary dissolved passageways and have water levels that are close to sea level but with the tidal cycle somewhat damped and lagged. Typically, the tidal

192 average range over a complete year is 0.5 m inside these caves compared to 0.8 m in the open
193 ocean (NOAA data), and lagged by ≈1-2 hours (Fig. S5).

194

195 Rainwater percolation to the karst water table creates brackish water lenses, resulting in lower
196 water density and therefore slightly higher water levels in caves than the ocean (e.g.(van
197 Hengstum et al., 2009)). Such deviations are expected to be very small, however. Water-table
198 gradients observed in the similar setting of the Yucatan, Mexico, are only 5–10 mm km^{-1}
199 (Marin and Perry, 1994), and the Bermuda caves of this study are less than 0.3 km from the
200 coast. Water levels in the caves can thus be considered as oscillating around the same
201 elevation as sea level (Boop et al., 2014).

202

203 **4. Materials and methods**

204 This study focuses on sample QB (Fig. 3), a stalactite 1.10 m long derived from a narrow
205 cave curtain hanging from a ceiling ~1.5 meters above sea level (masl, where sea level refers
206 to the present mean tide level) in Wilkinson Quarry Cave (Fig. 3 and S2). Most of the work
207 presented here was performed on two slices cut perpendicular to the growth axis at 1.37 (slice
208 B1Bi) and 1.28 (slice B1Cii) masl (Fig. 4, 5 and S1). The width of the sample is 6.5 cm at the
209 B1Cii slice (Fig. 4). XRD analyses demonstrate that the sample is calcite. It has a columnar
210 crystalline fabric, with the original stalactite composed of dense dark calcite (DCC). The
211 immediately subsequent growth-unit is composed of white porous calcite (WPC) with large
212 easily breakable crystals, with the remaining growth-units ranging from dark dense to milky
213 calcite.

214 Visual inspection of slices through the stalactite reveals five discontinuities (labelled D1 to
215 D5; Fig. 4, Tables 1 and S1), corresponding to possible hiatuses. Microscope inspection of
216 these discontinuities confirms the presence of perturbations in growth. The first of these, D1,
217 marks the boundary of the central soda-straw portion of growth from the rest of the stalactite
218 on B1Cii, with an abrupt change from DCC to WPC. Discontinuities D3 and D4 are
219 characterised by an abrupt change from DCC to a few millimetres of more porous calcite.
220 The same applies to D5 except that porous calcite is observed towards the exterior of the
221 sample. New generations of crystals with competitive growth are identified all along D2 and
222 in some places along D4. Thin clay layer deposits are visible at D3, 4 and 5 (Fig. 4).

223

224 Sixteen U-Th ages were performed to assess the chronology of the QB stalactite, and to
225 assess possible periods of hiatus. The locations of the subsamples used are reported relative
226 to a horizontal axis on the B1Cii slice, using petrographic features as a guide to compare data
227 from other slices (Fig. 5 and S1). Details of the U-Th methods broadly follow (Mason and
228 Henderson, 2010) and are given in the supplementary material. Ages are reported relative to
229 1950. An age-depth model was constructed using the OxCal-4-2 software (Ramsey, 2008),
230 which adds the constraint that all U-Th ages have to be in stratigraphic order (Fig. 5). The age
231 model is used to extrapolate the U-Th ages of samples from between growth boundaries to
232 ascertain the hiatus ages. The deposition rate is controlled using P_Sequences, assuming
233 random Poisson processes and allowing growth-rate fluctuations (see supp. mat. for detailed
234 parameters).

235 Samples from Walsingham Cave, Squeeze Cave, Admiral's Cave, Crystal Cave and others
236 from Wilkinson Quarry Cave, as well as pieces of flowstone retrieved from the shore cliff at
237 Camp St David, were also dated as part of this study. These samples ranged in height relative

238 to sea level from -14 to +12 m. They do not provide information used here to constrain sea
239 level, but the age of their growth is used in discussion of the sea-level results. Full details and
240 results for these other samples are provided in the Supplemental Material.

241

242 **5. Results**

243 All but one of the U-Th ages for the QB stalactite are in stratigraphic order within their dating
244 uncertainties (Table S1; Fig. 5). The sample grew from late MIS6 (141.5±2.2 ka) to late
245 MIS5a (72.9±1.4 ka). Notable steps in age are observed in the sample at depths
246 corresponding to D1 and D2, and possible steps also seen at D3 and D4 (Fig. 5). The OxCal
247 age-depth model provides a probabilistic assessment of the timing and duration of growth
248 hiatuses associated with these steps in age, with hiatuses starting at 137±5, 106±6, 84.3±1.5,
249 and 79.9±0.9 ka (Table 1), broadly correlating with the sea-level highstands of MIS5
250 recorded at other sites worldwide (e.g. Fig. 6), as recorded by the continuous Red Sea record
251 (Grant et al. 2012, Siddall et al., 2003).

252

253 A total of 61 dates were obtained on the 17 other samples from Wilkinson Quarry Cave,
254 Squeeze Cave, Crystal Cave, Walsingham Cave, Admiral's Cave and on flowstones of Camp
255 St David dated within this study (Table S2, Fig. S3). The growth episodes documented are
256 equally distributed during glacial, interglacial and intermediate climate episodes from MIS7
257 (Admiral's stalagmite, 216.0 ± 4 ka) to recent Holocene (Squeeze S3, 4.5 ± 1.1 ka). Holocene
258 and Termination I are the most represented probably due to easier access to this younger
259 period. Samples collected at greater depth (-14 m) grew during the last glacial. Growth

episodes during part of MIS7, MIS6, late MIS5b and MIS5a were documented in the highest sample, from +10 masl, the Admiral's Cave giant stalagmite.

6. Discussion

6.1. Are the four growth hiatuses due to sea-level rise?

The correlation of growth hiatuses (D1 to D4) with known periods of sea-level highstand suggest that flooding of stalagmite QB may be responsible for these hiatuses. Other possible explanations are a change in the local flow conditions in the cave, or a change in climate towards more arid conditions at these times.

A local change in the cave could be caused by an obstruction of the fissures upstream from this stalactite and/or a change in the water pathway in the epikarst. To explain the data, such a hydrological phenomenon would have had to occur repeatedly and then reverse, simultaneously with sea level changes, which seems unlikely. A change in cave ventilation or a vegetation cover degradation could also imply speleothem growth cessation but this would be detected in the carbon isotopic composition of the speleothem calcite ($\delta^{13}C_c$). As shown in figure 6 (d), there is no specific $\delta^{13}C_c$ range or pattern showing up repeatedly at each discontinuity and D2 and D3 are more likely to be associated with enhanced vegetation rather than degradation, as the $\delta^{13}C_c$ values decrease.

Alternatively, regional atmospheric events, such as modifications of the climatic pattern in the North Atlantic, could have led to aridification, causing speleothem growth interruptions across Bermuda. Aridification would be expected to cause a rise in Sr/Ca and Mg/Ca in the stalactite due to increasing prior calcite precipitation in the overlying karst, but no evidence

283 for such correlated increases either side of the hiatuses are observed in trace-metal data (Fig.
284 S7) arguing against changes in rainfall. There is also evidence for growth of speleothem at
285 greater height on Bermuda during one of the hiatuses (D1; Fig. 6, (Hearty et al., 1999))
286 indicating continued rainfall during that period. The hiatuses also do not correlate with
287 particular changes in temperature or ocean salinity (a crude proxy for rainfall) in the region.
288 They typically occur during warmer periods, which would likely favour more humid
289 conditions, but without any particular relationship to temperature changes in nearby sites (e.g.
290 Fig. 6), and salinity in the region is rather constant during the period studied here. Such
291 evidence makes it unlikely that the hiatuses are due to dry episodes on Bermuda. Such
292 periods of aridity are, in any case, not expected at Bermuda, which is located in the middle of
293 the Atlantic, where persistent Westerlies have likely provided constant moisture supply.
294 Climatic conditions are likely to have remained favourable to speleothem deposition at
295 Bermuda throughout MIS 5, and these four hiatuses are therefore unlikely to be the product
296 of episodic aridity.

297 An attempt to distinguish hiatuses caused by sea-level submersion from those due to other
298 causes by chemical fingerprinting was attempted in this study. We were hoping to find
299 increases in marine ions or a shift toward marine values in the stable isotope composition in
300 proximity to the sea-level related discontinuities, but none were visible at the resolution of
301 sampling we conducted (see Supplemental Material for further details, particularly Fig. S7).

302 The correspondence of hiatuses with known highstand periods, coupled to the continued
303 growth of speleothems at greater elevation in Bermuda and the lack of any other evidence for
304 changes in rainfall or vegetation, argues strongly that the breaks in growth relate to
305 submergence of the sample during sea-level highstands.

306 6.2 Implications for RSL reconstruction at Bermuda

307 The hiatuses dated in this study are continuous to the stump of the stalactite, requiring a
308 minimum RSL above the elevation of the ceiling from which it grew at +1.5±0.5 masl. RSL
309 is therefore above +1.5 masl at four times during MIS 5 (Table 1), correlating with MIS 5e,
310 MIS 5c, and two periods within MIS 5a, as shown in Figure 6. The 0.5 m uncertainty apply to
311 the elevation of the stump of the stalactite: the precision of this RSL reconstruction is
312 certainly a bit larger due to tides amongst others, but allows to circumvent the large depth
313 range associated to coral data reconstructions in the order of tens of meters (Hibbert et al.,
314 2016).

315 The duration of the hiatuses, computed using the OxCal age model, provides a possible
316 duration for the timespan when RSL was above +1.5 m for these four periods (Table S1)
317 although these must be considered maximum durations because of the remaining possibility
318 of periods where lack of growth is not due to flooding.

319 Sea-level above +1.5 m during MIS 5e comes as no surprise, with abundant observations
320 around the world placing eustatic sea level up to ≈+9 m above modern during this period (e.g.
321 Kopp et al., 2009, Dutton and Lambeck 2012, Dutton et al., 2015), and more limited data
322 indicating Bermudian RSL above modern (e.g. coral deposits at +4 to +6 m dated 126-
323 113 ka (Muhs et al., 2002) and 134 to 118 ka (Harmon et al., 1983), and marine aragonite on
324 speleothem at +3 to +4 m growing from ~130-110 ka (Harmon et al., 1978)) (Fig. 2).

325 That Bermudian RSL was above +1.5 m during MIS 5c and MIS 5a was previously unclear,
326 and the new constraints from this study contribute significantly to the controversy about high-
327 stand amplitude for these periods (e.g. Fig. 2). The MIS 5c hiatus encompasses the ages of
328 MIS5c coral fragment ages obtained by Harmon et al. (1978, 1983), and the MIS 5a hiatuses
329 encompass ages of coral fragments and geomorphological evidence for highstand (Harmon et
330 al. (1978, 1983), Vacher and Hearty (1989), Hearty et al. (1992), Ludwig et al. (1996) and

331 Muhs et al. (2002)). These correlations support the view that, although none of the dated
332 coral fragments are in life position, they are nevertheless found in sediments that formed
333 close to modern sea level.

334 Hiatuses in speleothem growth in this study argue against previous indications for lower sea
335 level during MIS5c and 5a in speleothem data by Harmon et al. (1981,1983), suggesting that
336 these early studies lacked the precision and resolution of U-Th dating to reveal period of
337 growth hiatus in the submerged sample.

338 The new data from this study provide strong evidence for Bermudian RSL above modern at
339 MIS5c and MIS5a. Observations at other locations around the world place RSL significantly
340 below modern at MIS5c and MIS5a. Such observations are not at odds with those presented
341 here, but indicate the important role of isostatic adjustment in controlling the pattern of RSL,
342 and the location of Bermuda on the glacial forebulge. New confidence in Bermudian RSL at
343 MIS5c and 5a will help to constrain the history of this forebulge in relation to earth properties
344 and ice-loading.

345

346 6.3. Multiple rises during MIS5

347 Two growth interruptions on the QB stalactite are documented during the MIS5a: from
348 84.3±1.5 to 82.0±1.1 ka and from 79.9±0.9 to 75.0±0.8 ka (referred as MIS5a' in Fig. 4,
349 Tables 1 and S3, Fig. 6). The earlier of these is short (2.4±1.8 ka, Table 1) and less clear in
350 the texture of the sample but, if taken at face value, the data suggests the presence of two
351 peaks in RSL. Such a pattern of sea level is consistent, within uncertainty, with the MIS5a
352 Bermudian coral ages obtained by Muhs et al. (2002), and with the timing of the two first
353 MIS5a sea-level rises of the Red Sea record (Fig. 6).

354 Previous studies suggesting a double highstand at MIS5a have been from tectonically active
355 regions (e.g. (Dumas et al., 2006; Potter et al., 2004; Surić et al., 2009)), allowing the
356 possibility that tectonic movements might drive observed RSL changes. The tectonic stability
357 of Bermuda makes it very unlikely that the double RSL peak observed in this study can be
358 explained by tectonic movement. This oscillation therefore appears likely to be due to a
359 change in ice volume and therefore a global feature.

360

361

362 6.4 Illustration of constraints for glacial isostatic adjustment modelling

363 Bermudian RSL is characterised by highstands above modern at each of MIS5e, 5c and 5a.
364 This contrasts with sites from further south, which experience significantly lower highstands
365 at MIS5c and 5a (Fig. 7). There is a clear RSL gradient from the forebulge sites such as
366 Bermuda to the more far-field sites during these later MIS 5 highstands. Potter and Lambeck
367 (2003) explained this contrasting behaviour with glacio-isostatic adjustment (GIA), testing
368 specific changes in ice sheet geometry and Earth model parameters.

369 To illustrate the constraints that the data can place on the GIA models, we explore predictions
370 for the Bermudian highstands from a set of GIA models tuned to reproduce the Red Sea RSL
371 curve (Williams, 2016). The independent chronology (Grant et al., 2012) and continuous
372 nature of the Red Sea RSL curve make it a good candidate for developing ice volume
373 histories, and it has been a target for several such GIA modelling studies. Details of the GIA
374 modelling and ice sheet development used in this study can be found in the Supplementary
375 Material. While the following results cannot be considered a new model based on or tuned to

376 the Bermudian data, they serve to illustrate the ability of GIA to cause the characteristic RSL
377 gradients seen to extend across the WNAC region during MIS 5c and MIS 5a.

378 GIA model results depend on the ice history and Earth model parameters used in the model
379 run, both of which are uncertain. We explore how Bermudian highstand data could constrain
380 the range of values that are realistic for these important model inputs. We developed two ice
381 histories with differing ice-dispersal templates. ICE 1 has an ice-dispersal template based on
382 ICE-5G (Peltier, 2004) whereas ICE 2 has a template based on a 3-D algorithmic ice model
383 (de Boer et al., 2014) (see Supplementary Material). The different dispersal templates result
384 in differing locations and thicknesses of ice, as well as changes in individual ice-sheet
385 volumes. We then explored, with a series of model runs, the effect of a range of Earth model
386 parameters (i.e. the upper- and lower-mantle viscosity) on the model predictions (Fig. 8). The
387 range of upper- and lower-mantle viscosity values in Figure 8 is sampled by 165 different
388 sets, and this range of values encompasses the values considered in Potter and Lambeck
389 (2003).

390 Most values of model parameters do not produce RSL above modern for all three MIS5
391 highstands at Bermuda, illustrating the ability of the data to constrain these input parameters.
392 Models with high values of lower mantle viscosity (typically $>3x10^{22}$ Pa s), and upper mantle
393 viscosity values of about 2 to $5x10^{20}$ Pa s, result in predictions of all three highstands being
394 close to modern (Fig. 8). This subset of viscosity values are rather similar to those found to
395 yield the best results by Potter and Lambeck, 2003. A slow solid-Earth response to rapid
396 changes of sea level during MIS5, generated by high lower-mantle viscosity, allows RSL at
397 Bermuda to be above modern, while global mean sea level is much lower by the end of MIS
398 5a.

399 Ice distribution also plays an important role in the RSL response at Bermuda, with ICE 2
400 generally producing a more consistent set of maxima near present-day values for this set of
401 Earth models (Fig. 8). A key difference between ice dispersal models is that the Laurentide
402 ice sheet is smaller in ICE 2 than in ICE 1 during MIS 6, supporting the conclusions of Potter
403 and Lambeck (2003), who found that a small, northerly North American ice sheet was
404 suggested by available sea-level data.

405 The GIA modelling described here demonstrates the possibility to fit the gradient of sea-level
406 change across the WNAC region during MIS 5 (e.g. Fig. 9) with RSL close to modern three
407 times at Bermuda, but significantly lower in MIS5c and 5a further south (e.g. Yucatan and
408 Barbados). The fit between models and data is not perfect, indicating the continued need for
409 refinement in ice-sheet loads and earth properties in GIA models. We also note that Potter
410 and Lambeck (2003) suggested that different values of upper mantle viscosity may be needed
411 to successfully model observations in Bermuda versus the rest of the WNAC region, i.e. there
412 must be lateral variations in upper mantle viscosity to explain the results. That RSL is above
413 modern during each of MIS5e, 5c and 5a at Bermuda provides a powerful observational
414 constrain for such future modelling, and will help to further understand ice-loading and
415 forebulge evolution through time.

416

417 **7. Conclusion**

418

419 This speleothem study reveals relative sea-level variation history during MIS5 at Bermuda, a
420 site located on the forebulge created by ice-loading during glacial periods. Based on
421 speleothem U-Th ages, relative sea level was higher than 1.5±0.5 masl during the Last
422 Interglacial highstand of MIS 5e and also during MIS5c and MIS5a, providing precise ages

for these previously controversial later highstands. The results also suggest a double RSL rise at MIS5a, supporting previous evidence of a rapid sea level variation for this period and, given the tectonic stability of Bermuda, suggesting this is a global feature associated with changes in ice-sheet volume. Testing GIA models against these new constraints reinforces Potter and Lambeck's (2003) conclusions suggesting the presence of a smaller, northerly-based Laurentide ice sheet during the later MIS 5 and a restricted range of Earth viscosity values, with higher values of lower-mantle viscosity than are used in some GIA models of the Last Interglacial. That Bermudian sea level was above modern during MIS5c and 5a provides powerful constraints for future GIA models to help refine ice-sheet histories and Earth properties. It also demonstrates, more generally, the potential for highstands at this setting to be significantly higher than in other regions, helping to explain high sea level data for Bermuda from earlier highstands.

Acknowledgements

We are grateful to D. Summers who, as representative of the Wilkinson Estate, granted permission for access to the Wilkinson's Quarry Cave. G. Nolan and A. Mello are to be thanked for the invaluable assistance they provided to M. Rowe in the collection of speleothems from Wilkinson's Quarry Cave. We thank C. Bronk Ramsey for his help in improving the age model, P. Holdship, C.C. Day, A. Hsieh for helping with trace metals, stable isotopes, U-Th measurements. D. Samson is thanked for his help in improving the figures and O. Green for the thin section preparation. XRD analyses were done at GSI in collaboration with A. Ayalon and M. Bar-Matthews. We are also grateful to D. Ford and H. Schwarcz for providing the Crystal cave samples and to R. Smith and D. Petit at the

447 Government of Bermuda for delivering both sampling and export permit and R. Chandler for
448 his help in obtaining it. The National Museum of Scotland kindly provided access to samples
449 from the Admiral's Cave. This work was supported by the NERC NE/1008861/1 and
450 NE/I008365/1 (both iGlass). This is the Bermuda Biodiversity Project Contribution number
451 XXX.

452

453 **Fig and table captions**

454 Table 1

455 Characteristics of the discontinuities in sample QB. Ages and uncertainties are based on the
456 OxCal modelling of new U-Th age data of this study.

457 Figure 1: Location map of Bermuda in the Western North-Atlantic Caribbean geodynamic
458 context. The forebulge effect is visible through the colour shading representing the numerical
459 prediction of the modern day impact of glacio-isostatic adjustment on relative sea level in
460 mm/yr (adapted from Tamisiea and Mitrovica, 2011). Sites indicated in black are those for
461 which RSL at MIS 5e, c, and a have been documented and are used in the discussion. Sites
462 indicated in blue are those from which marine data is used for comparison.

463 Figure 2: Summary of the relevant RSL data available for the MIS5 at Bermuda. Note the
464 disagreement existing for the RSL at MIS5c and 5a.

465 Figure 3: Picture of the QB stalactite in Wilkinson Quarry Cave. The ceiling is at 1.5±0.5m
466 above the mean tidal height of the surface of the cave pool.

467 Figure 4: Polished section of slice B1Cii from the QB stalactite and cross-polar light
468 microscope images from vicinity of discontinuity D1 to D4.

Figure 5: Slices B1Cii and B1Bi from sample QB and corresponding U-Th results. a) views perpendicular to the growth axis for B1Bi and B1Cii, . b) U-Th ages with black diamonds standing for the sub-samples collected on B1Cii.Grey ones are from B1Bi. The youngest white diamonds is from B2, while the other white one is from B3. 95% probability error bars are reported. c) OxCal age model: Black diamonds represent all U-Th ages as in Table S1. Black line is the mean age model curve, grey lines represent the 95% probability envelope, and grey circles are for growth boundaries, all computed from the OxCal model (Ramsey, 2008). Only one U-Th date, in the second deposition unit, was considered as an outlier and was rejected. This "adopted" model was obtained using a 5 Poisson sequences deposition model, each sequence corresponding to a growth unit, limited by a growth hiatus. See supplementary material for more details. Four hiatuses appear as steps in the age model.

Figure 6: Comparison of QB growth episodes (discontinuities shown by vertical grey bars) with other data from QB and nearby marine records. a) QB growth periods, with 2σ uncertainty on the boundaries deduced from OxCal model (Fig. 5 and Table S3). The continuous RSL for the Red-Sea (Grant et al., 2012; Siddall et al., 2003) is shown for comparison to allow recognition of highstands identifying the very different isostatic response at this site which is far field and therefore minimally impacted by ice loading/unloading. The comparison is made to the Red Sea sea-level record because it is to date one of the most accepted reference as it is one of the most complete record and because of its independent chronology. Also shown are isolated dates from speleothems at greater altitude on Bermuda than QB.; b) UK'_{37} sea-surface temperature from MD95-2036 (Grant et al., 2013; Lehman et al., 2002); c) $\delta^{18}O_{ivf\text{-}sw}$ of *G. ruber (w)* and *G. truncatulinoides (s)* representing salinity from ODP Site 1058 (Bahr, et al., 2013; Figure 1 for location); (d) $\delta^{13}C$ and (e) $\delta^{18}O$ of the QB speleothem carbonate along a radial transect across B1Cii (this study).

493 Figure 7: Summary of RSL observations across the WNAC region including results in this
494 study at MIS5e (red), 5c (green), and 5a (black), adapted from Potter and Lambeck, 2003.
495 Symbols are used either when the RSL estimation is at a specific elevation or indicate the
496 position of the indicator for a minimum or a maximum RSL (for instance the depth of a
497 stalagmite that stopped growing.) Rectangles represent range of positions the RSL might
498 have reached. In the absence of a RSL upper limit, rectangles are interrupted arbitrarily at
499 +10m. Shadings indicate the regional trend for each period. Data are provided for the US
500 Atlantic coastal plain (ACP, Cronin et al. 1981; Wehmiller et al., 2004), Bermuda (BDA,
501 Harmon et al., 1978, 1983, Vacher et al., 1989, Muhs et al., 2002, this study empty circle),
502 Grand Bahama (GB, Lundberg and Ford, 1994, Richards et al., 1994), the Florida Keys (FK,
503 Ludwig et al., 1996; Toscano and Lundberg, 1999), Haiti (Dodge et al., 1983; Dumas et al.,
504 2006), Yucatan, Mexico (Yuc, Moseley et al., 2013), Grand Cayman Island (Cay, Coyne et
505 al., 2007) and Barbados (Bar, e.g. Radtke and Schellmann, 2005 as a review). Data from
506 tectonically active places include uplift correction as provided by the authors. While
507 consistent during MIS5e, a RSL gradient from inner bulge to far-field sites appear for the
508 MIS5a and MIS5c highstands.

509 Figure 8: GIA model predictions of maximum RSL at Bermuda during MIS5e, 5a, and 5c
510 using constant lithospheric thickness of 96 km and varying upper and lower mantle viscosity
511 values. Each plot shows the variation of the maximum predicted sea level during each of the
512 interstadials (columns for MIS 5e, 5c and 5a) as contours versus changes in the Earth model's
513 upper (y axis) and lower (x axis) mantle viscosity values. The rows present the results for the
514 two different ice models used in the modelling.

515 Figure 9: GIA model predictions for RSL at Bermuda, the Yucatan and Barbados and Global
516 Mean Sea Level (GMSL) used for these predictions using the ICE 2 model (equivalent results
517 for ICE 1 show similar variations, a couple of meters higher). RSL histories using ICE 2 and

an Earth model with a lithospheric thickness of 96 km, an upper mantle viscosity of $4x10^{20}$ Pa s and a lower mantle viscosity of $3x10^{22}$ Pa s are presented. Note that the three locations in the WNAC region demonstrate different behaviour, especially for 5a and 5c.

References

Boop, L.M., Onac, B.P., Wynn, J.G., Fornós, J.F., Rodríguez-Homar, M., Merino, A., 2014. Groundwater geochemistry observations in littoral caves of Mallorca (western Mediterranean): implications for deposition of phreatic overgrowths on speleothems. International Journal of Speleology 43, 193-203.

Coyne, M.K., Jones, B., Ford, D., 2007. Highstands during Marine Isotope Stage 5: evidence from the Ironshore Formation of Grand Cayman, British West Indies. Quaternary Sci Rev 26, 536-559.

Cronin, T.M., Szabo, B.J., Ager, T.A., Hazel, J.E., Owens, J.P., 1981. Quaternary Climates and Sea Levels of the U.S. Atlantic Coastal Plain. Science 211, 233-240.

de Boer, B., Stocchi, P., van deWal, R.S.W., 2014. A fully coupled 3-D ice-sheet–sea-level model: algorithm and applications. Geoscientific model development 7, 2141-2156.

Dodge, R.E., Fairbanks, R.G., Benninger, L.K., Maurrasse, F., 1983. Pleistocene Sea Levels from Raised Coral Reefs of Haiti. Science 219, 1423-1425.

Dumas, B., Hoang, C.T., Raffy, J., 2006. Record of MIS 5 sea-level highstands based on U/Th dated coral terraces of Haiti. Quatern Int 145, 106-118.

Dutton, A., Lambeck, K., 2012. Ice Volume and Sea Level During the Last Interglacial. Science 337, 216-219.

Dutton, A., Webster, J.M., Zwartz, D., Lambeck, K., Wohlfarth, B., 2015. Tropical tales of polar ice: evidence of Last Interglacial polar ice sheet retreat recorded by fossil reefs of the granitic Seychelles islands. Quaternary Sci Rev 107, 182-196.

Grant, J., Hopcraft, C., Borner, M., Haydon, D.T., 2013. Revived species: where will they live? Nature 493, 608-608.

Grant, K.M., Rohling, E.J., Bar-Matthews, M., Ayalon, A., Medina-Elizalde, M., Ramsey, C.B., Satow, C., Roberts, A.P., 2012. Rapid coupling between ice volume and polar temperature over the past 150,000 years. Nature 491, 744-747.

Harmon, R.S., Land, L.S., Mitterer, R.M., Garrett, P., Schwarcz, H.P., Larson, G.J., 1981. Bermuda Sea-Level during the Last Interglacial. Nature 289, 481-483.

Harmon, R.S., Mitterer, R.M., Kriausakul, N., Land, L.S., Schwarcz, H.P., Garrett, P., Larson, G.J., Vacher, H.L., Rowe, M., 1983. U-Series and Amino-Acid Racemization Geochronology of Bermuda -

Implications for Eustatic Sea-Level Fluctuation over the Past 250,000 Years. Palaeogeogr Palaeocl 44, 41-70.
Harmon, R.S., Schwarcz, H.P., Ford, D.C., 1978. Late Pleistocene sea level history of Bermuda. Quaternary Res 9, 205-218.
Hearty, P.J., 2002. Revision of the late Pleistocene stratigraphy of Bermuda. Sediment Geol 153, 1-21.
Hearty, P.J., Kindler, P., 1995. Sea-Level Highstand Chronology from Stable Carbonate Platforms (Bermuda and the Bahamas). J Coastal Res 11, 675-689.
Hearty, P.J., Kindler, P., Cheng, H., Edwards, R.L., 1999. A +20 m middle Pleistocene sea-level highstand (Bermuda and the Bahamas) due to partial collapse of Antarctic ice. Geology 27, 375-378.
Hearty, P.J., Vacher, H.L., Mitterer, R.M., 1992. Aminostratigraphy and Ages of Pleistocene Limestones of Bermuda. Geological Society of America Bulletin 104, 471-480.
Heusser, L., Oppo, D., 2003. Millenial- and orbital-scale climate variability in southeastern United States and in the subtropical Atlantic during Marine Isotope Stage 5: evidence from pollen and isotopes in ODP Site 1059. Earth Planet Sc Lett 214, 483-490.
Hibbert, F.D., Rohling, E.J., Dutton, A., Williams, F.H., Chutcharavan, Cheng Zhao P.M, Tamisiea, M.E., 2016. Coral indicators of past sea-level change: A global repository of U-series dated benchmarks. Quatrenary science reviews 145, 1-56.
Horton, B.P., Peltier, W.R., Culver, S.J., Drummond, R., Engelhart, A.C., Kemp, A.C., Mallinson, D., Thieler, E.R., Riggs, S.R., Ames, D.V., Thomson, K.H., 2009. Holocene sea-level changes along the North Carolina Coastline and their implications for glacial isostatic adjustment models. Quaternary science review 28, 1725-1736.
Kendall, R.A., Mitrovica, J.X., Milne, G.A., 2005. On post-glacial sea level -- II. Numerical formulation and comparative results on spherically symmetric models. Geophys J Int 161, 679-706.
Kopp, R.E., Simons, F.J., Mitrovica, J.X., Maloof, A.C., Oppenheimer, M., 2009. Probabilistic assessment of sea level during the last interglacial stage. Nature 462, 863-U851.
Lambeck, K., Chappell, J., 2001. Sea Level Change Through the Last Glacial Cycle. Sci Technol Adv Mat 292.
Lambeck, K., Purcell, A., Flemming, N.C., Vita-Finzi, C., Alsharekh, A.M., Bailey, G.N., 2011. Sea level and shoreline reconstructions for the Red Sea: isostatic and tectonic considerations and implications for hominin migration out of Africa. Quaternary Sci Rev 30, 3542-3574.
Land, L.S., Mackenzi.Ft, Gould, S.J., 1967. Pleistocene History of Bermuda. Geol Soc Am Bull 78, 993-&.
Lehman, S.J., Sachs, J.P., Crotwell, M.A., Keigwin, L.D., Boyle, E.D., 2002. Relation of subtropical Atlantic temperature, high-latitude ice rafting, deep water formation, and European climate 130,000-60,000 year ago. Quaternary Sci Rev 21, 1917-1924.
Ludwig, K.R., Muhs, D.R., Simmons, K.R., Halley, R.B., Shinn, E.A., 1996. Sea-level records at 80 ka from tectonically stable platforms: Florida and Bermuda. Geology 24, 211-214.
Lundberg, J., Ford, D.C., 1994. Late Pleistocene Sea-Level Change in the Bahamas from Mass-Spectrometric U-Series Dating of Submerged Speleothem. Quaternary Sci Rev 13, 1-14.
Marin, L.E., Perry, E.C., 1994. The hydrogeology and contaminant potential of northwestern Yucatan, Mexico. Geofis International 33, 619–623.
Mason, A.J., Henderson, G.M., 2010. Correction of multi-collector-ICP-MS instrumental biases in high-precision uranium-thorium chronology. Int J Mass Spectrom 295, 26-35.
Meischner, D., Vollbrecht, R., Wehmeyer, D., 1995. Pleistocene seal evel yo– yo recorded in stacked beaches, Bermuda south shore. Geological Society of America Special Paper 300, 295–310.
Moseley, G.E., Smart, P.L., Richards, D.A., Hoffmann, D., 2013. Speleothem constraints on marine isotope stage (MIS) 5 relative sea levels, Yucatan peninsula, Mexico. Journal Of Quaternary Science.
Muhs, D.R., Simmons, K.R., Steinke, B., 2002. Timing and warmth of the Last Interglacial period: new U-series evidence from Hawaii and Bermuda and a new fossil compilation for North America. Quaternary Sci Rev 21, 1355-1383.

Peltier, W.R., 2004. Global glacial isostasy and the surface of the Ice-age Earth: the ICE-5G (VM2) Model and GRACE. Annual Review of Earth and Planetary Sciences 32.
Potter, E.K., Esat, T.M., Schellmann, G., Radtke, U., Lambeck, K., McCulloch, M.T., 2004. Suborbital-period sea-level oscillations during marine isotope substages 5a and 5c. Earth Planet Sc Lett 225, 191-204.
Potter, E.K., Lambeck, K., 2003. Reconciliation of sea-level observations in the Western North Atlantic during the last glacial cycle. Earth Planet Sc Lett 217, 171-181.
Radtke, U., Schellmann, G., 2005. Timing and magnitude of sea level change during MIS 5 derived from Barbados coral reef terraces: A critical literature review and new data. J Coastal Res, 52-62.
Ramsey, C.B., 2008. Deposition models for chronological records. Quaternary Sci Rev 27, 42-60.
Raymo, M.E., Mitrovica, J.X., 2012. Collapse of polar ice sheets during the stage 11 interglacial. Nature 483.
Richards, D., Smart, P.L., Edwards, R.L., 1994. Maximum sea levels for the last glacial period from U-series ages of submerged speleothems. Nature 367.
Rowe, M.P., Wainer, K.A.I., Bristow, C.S., Thomas, A.L., 2014. Anomalous MIS 7 sea level recorded on Bermuda. Quaternary Sci Rev 90, 47-59.
Siddall, M., Rohling, E.J., Almogi-Labin, A., Hemleben, C., Meischner, D., Schmelzer, I., Smeed, D.A., 2003. Sea-level fluctuations during the last glacial cycle. Nature 423, 853-858.
Surić, M., Richards, D.A., Hoffmann, D.L., Tibljaš, D., Juračić, M., 2009. Sea-level change during MIS 5a based on submerged speleothems from the eastern Adriatic Sea (Croatia). Mar Geol 262, 62-67.
Tamisiea, M.E., Mitrovica, J.X., 2011. The Moving Boundaries of Sea Level Change Understanding the Origins of Geographic Variability. Oceanography 24, 24-39.
Toscano, M.A., Lundberg, J., 1999. Submerged Late Pleistocene reefs on the tectonically-stable S.E. Florida margin: high-precision geochronology, stratigraphy, resolution of Substage 5a sea-level elevation, and orbital forcing. Quaternary Sci Rev 18, 753-767.
Vacher, H.L., Hearty, P., 1989. History of Stage-5 Sea-Level in Bermuda - Review with New Evidence of a Brief Rise to Present Sea-Level during Substage-5a. Quaternary Sci Rev 8, 159-168.
Van Hengstum, P., Richards, D.A., Onac, B.P., Dorale, J.A., 2015. Coastal Caves and Sinkholes. In: Handbook for Sea-level Research (Shennan, I., Long, A., Horton, B., Eds.), John Wiley & Sons, Oxford, p. 83-103.).
van Hengstum, P.J., Scott, D.B., Javaux, E.J., 2009. Foraminifera in elevated Bermudian caves provide further evidence for +21 m eustatic sea level during Marine Isotope Stage 11. Quaternary Sci Rev 28, 1850-1860.
Vollbrecht, R., 1990. Marine and meteoric diagenesis of submarine Pleistocene carbonates from the Bermuda carbonate platform. Carbonates Evaporites 5, 13–95.
Wehmiller, J.F., Simmons, K.R., Cheng, H., Edwards, R.L., Martin-McNaughton, J., York, L.L., Krantz, D.E., Shen, C.C., 2004. Uranium-series coral ages from the US Atlantic Coastal Plain - the "80 ka problem" revisited.
Williams, F.H., 2016. A geophysical approach to reconstructing past global mean sea levels using highly resolved sea-level records. PhD Thesis, University of Southampton.

Figure1

Click here to download high resolution image

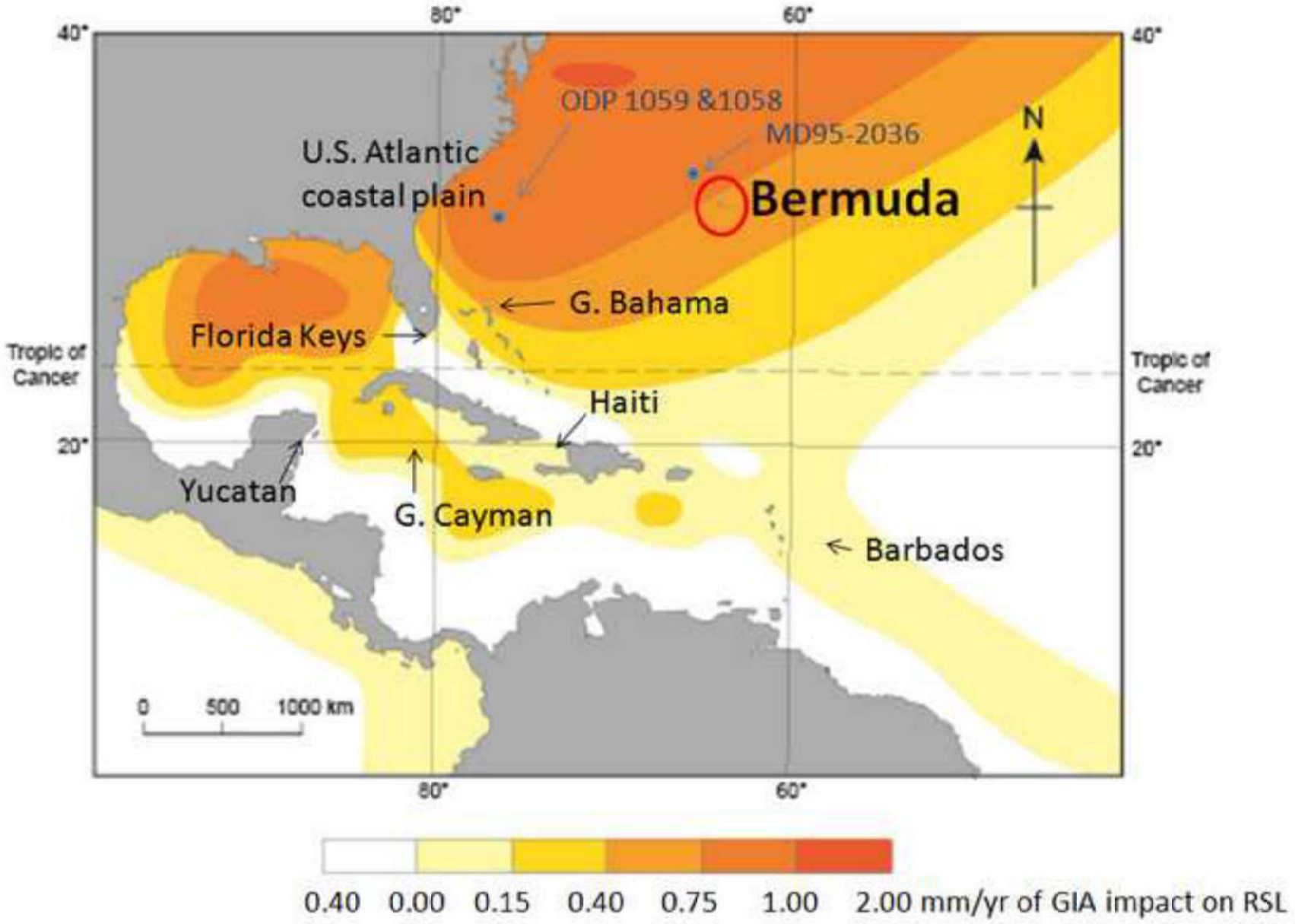

Figure2

Click here to download high resolution image

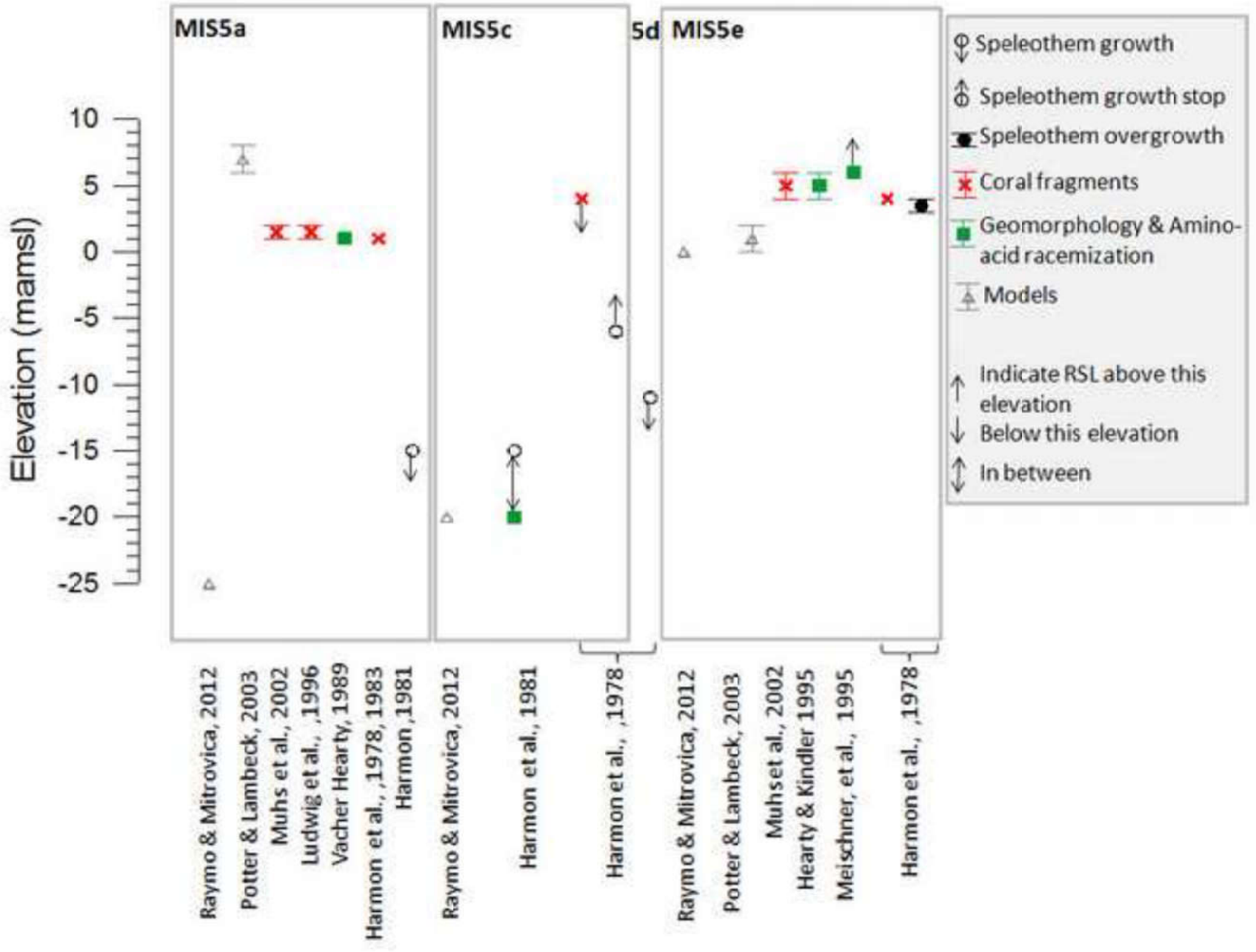

Figure3

Click here to download high resolution image

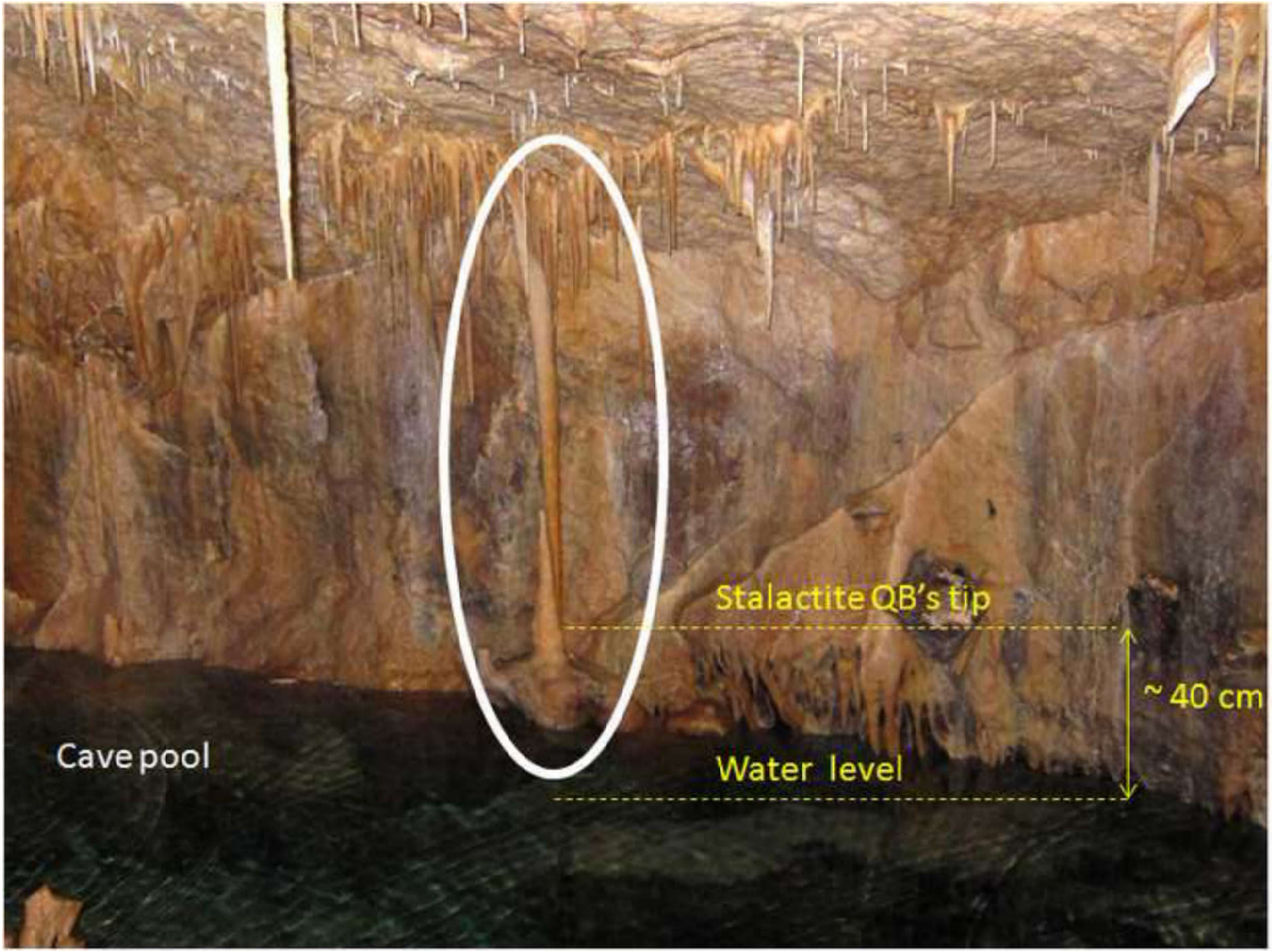

Figure4

Click here to download high resolution image

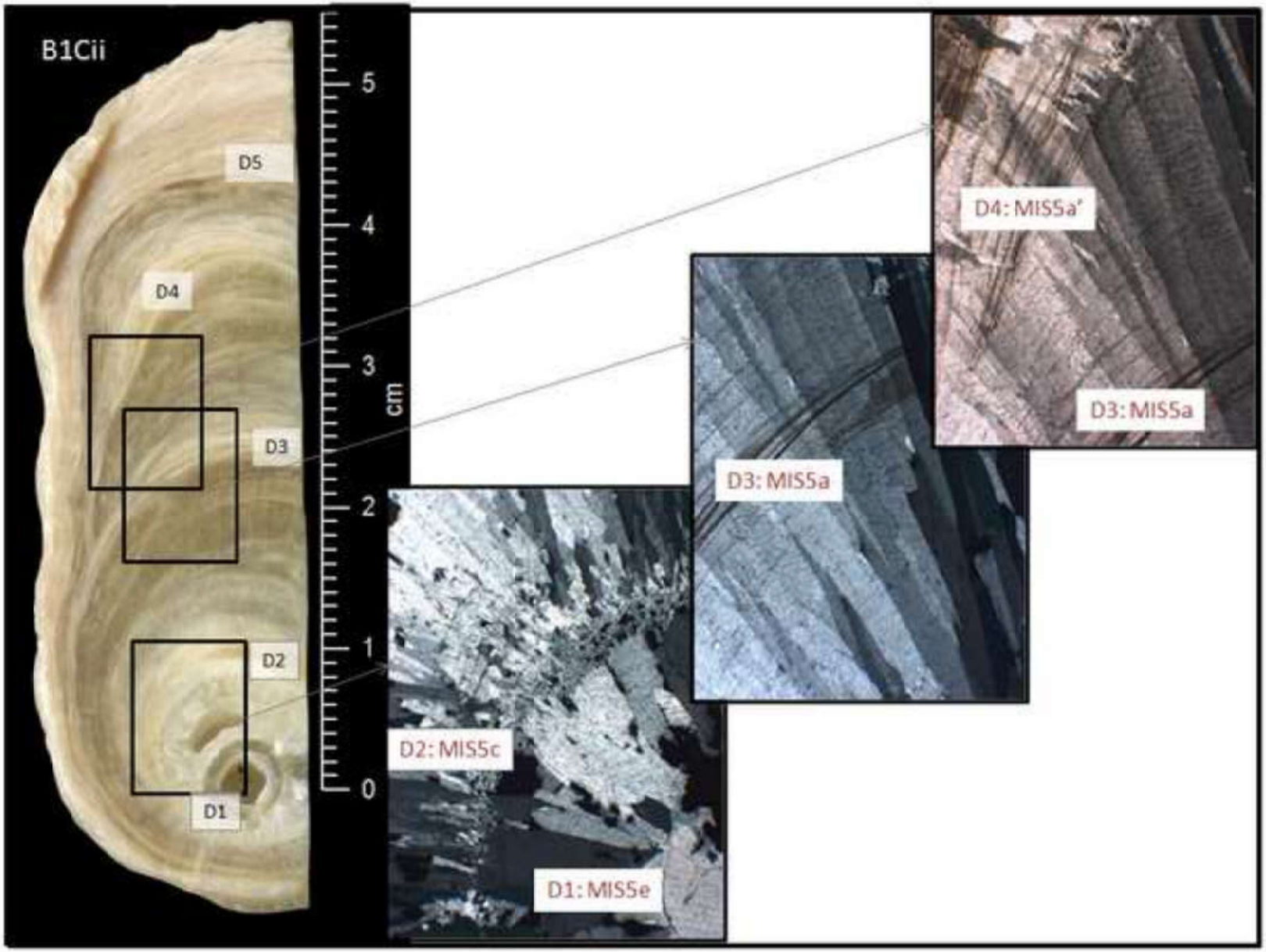

Figure5

Click here to download high resolution image

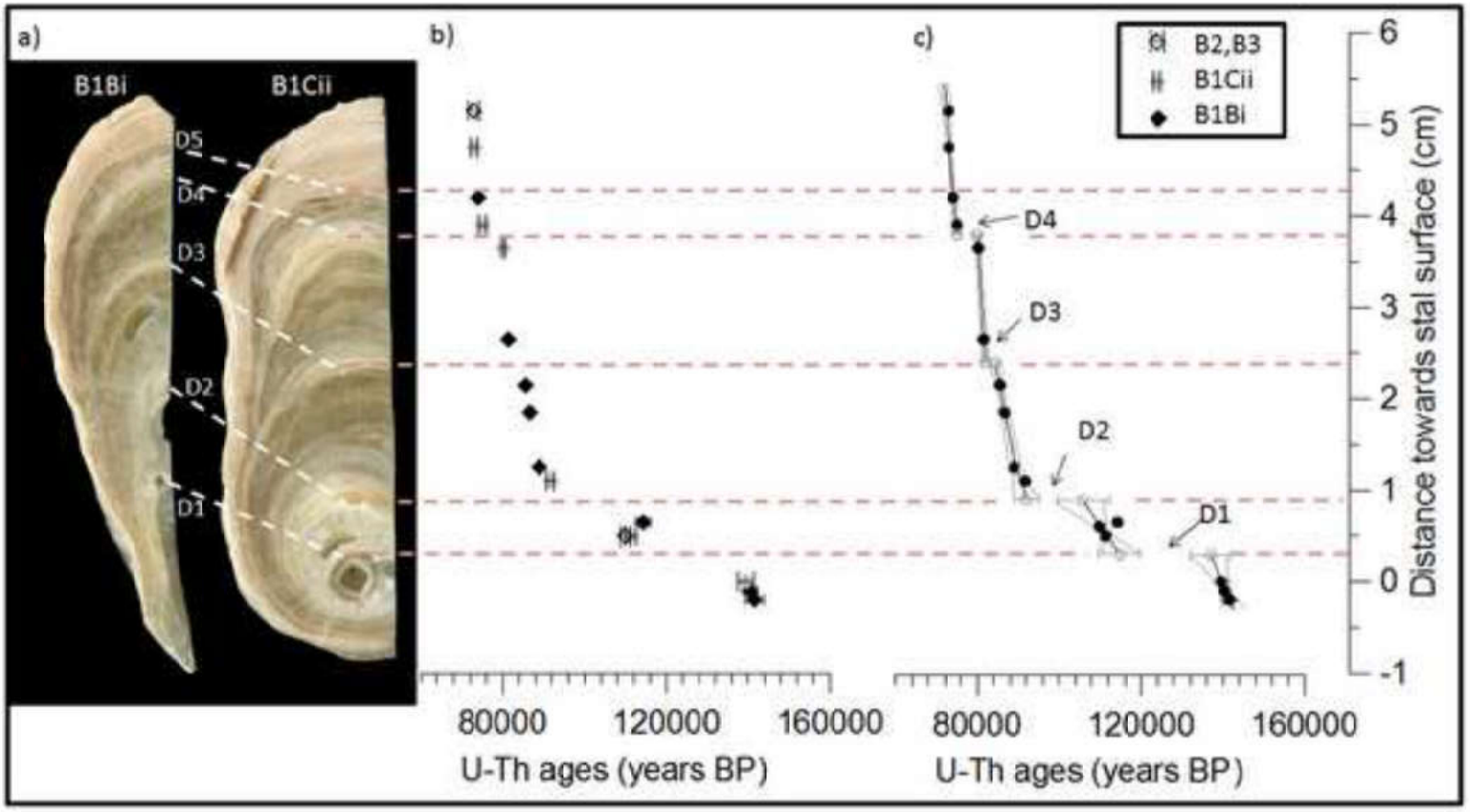

Figure6

Click here to download high resolution image

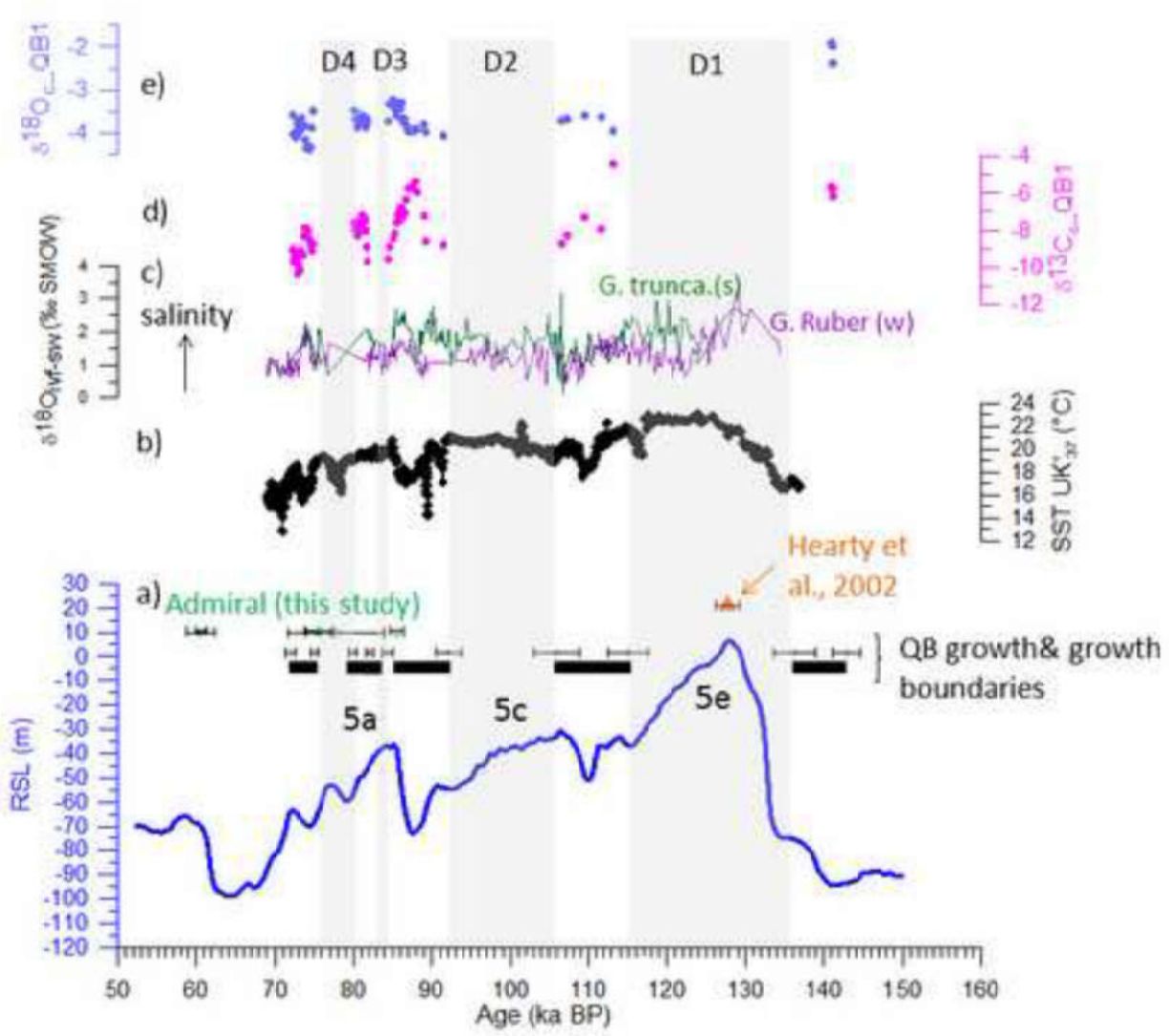

Figure7

Click here to download high resolution image

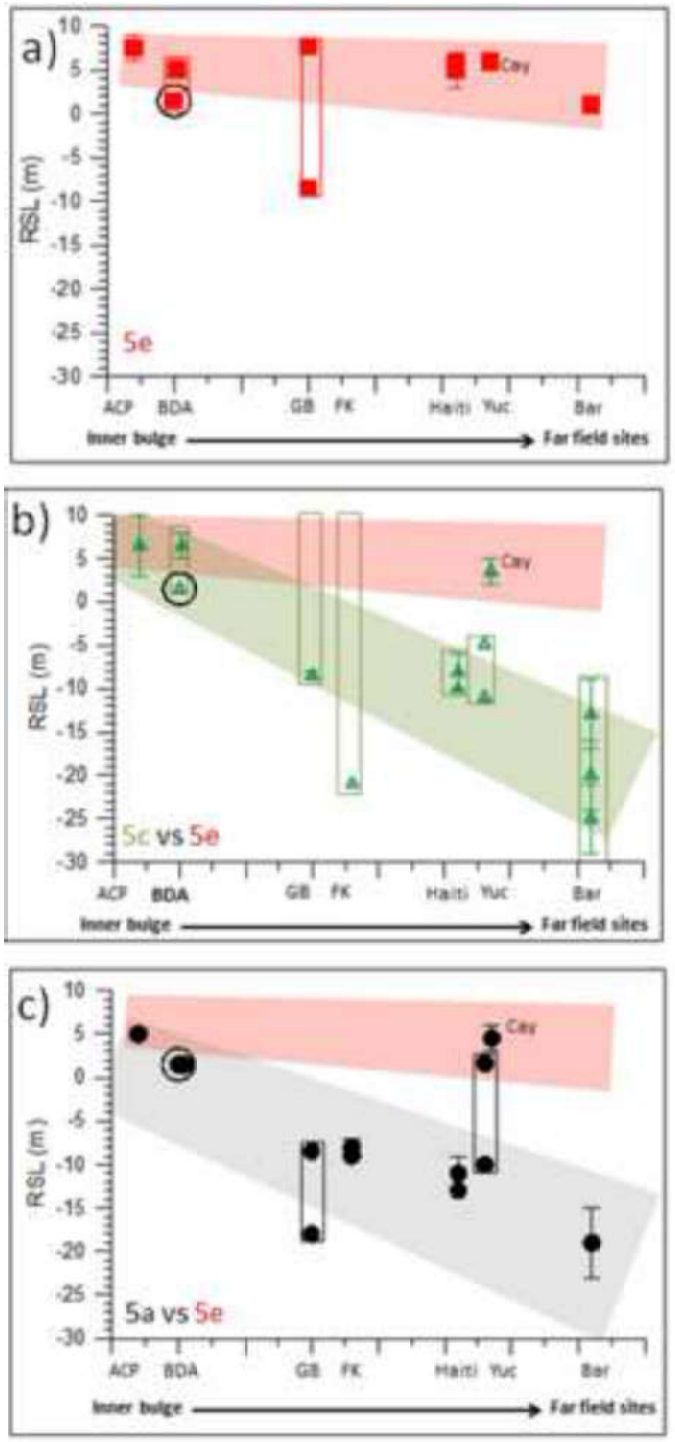

Figure 7

Figure8

Click here to download high resolution image

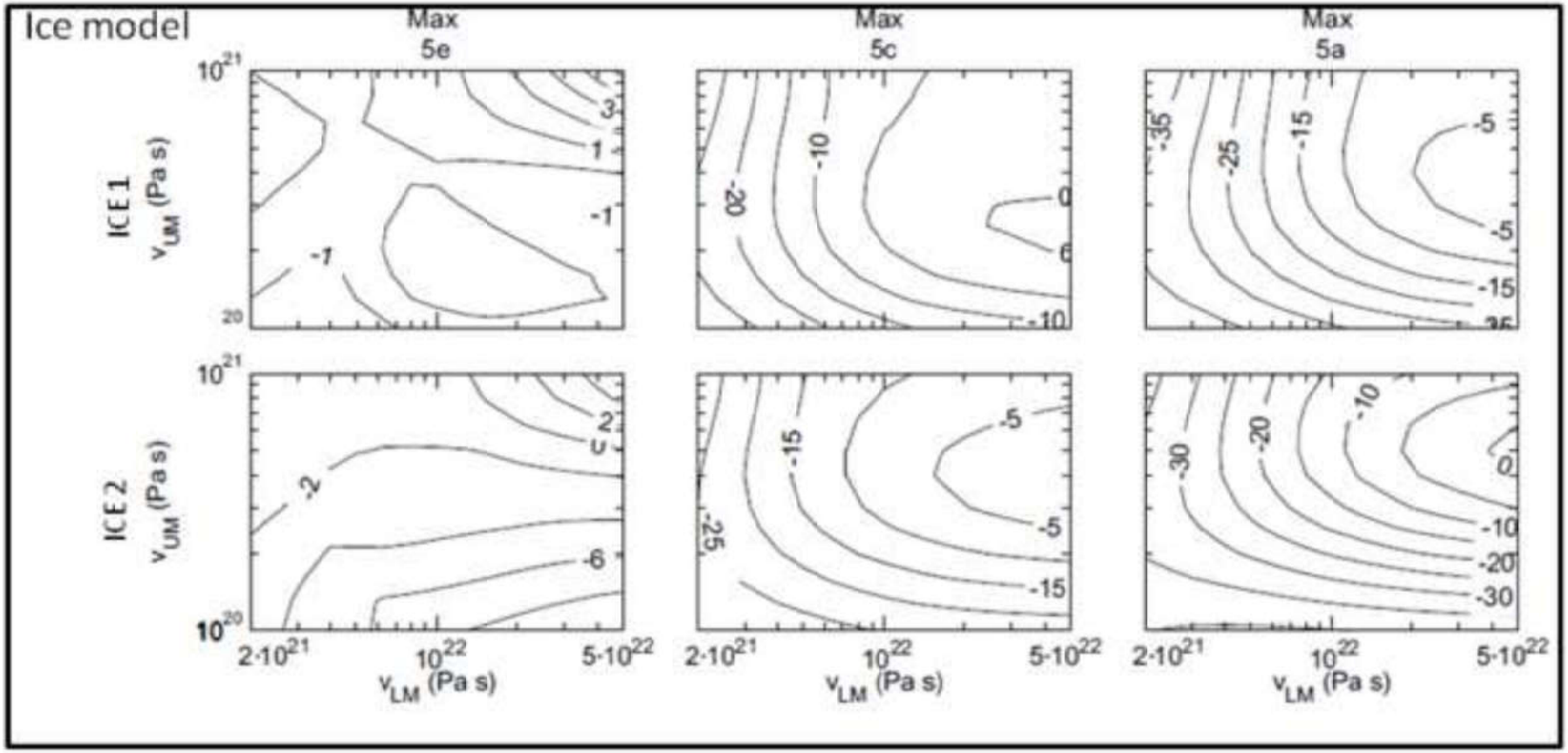

Figure 8

Figure9
Click here to download high resolution image

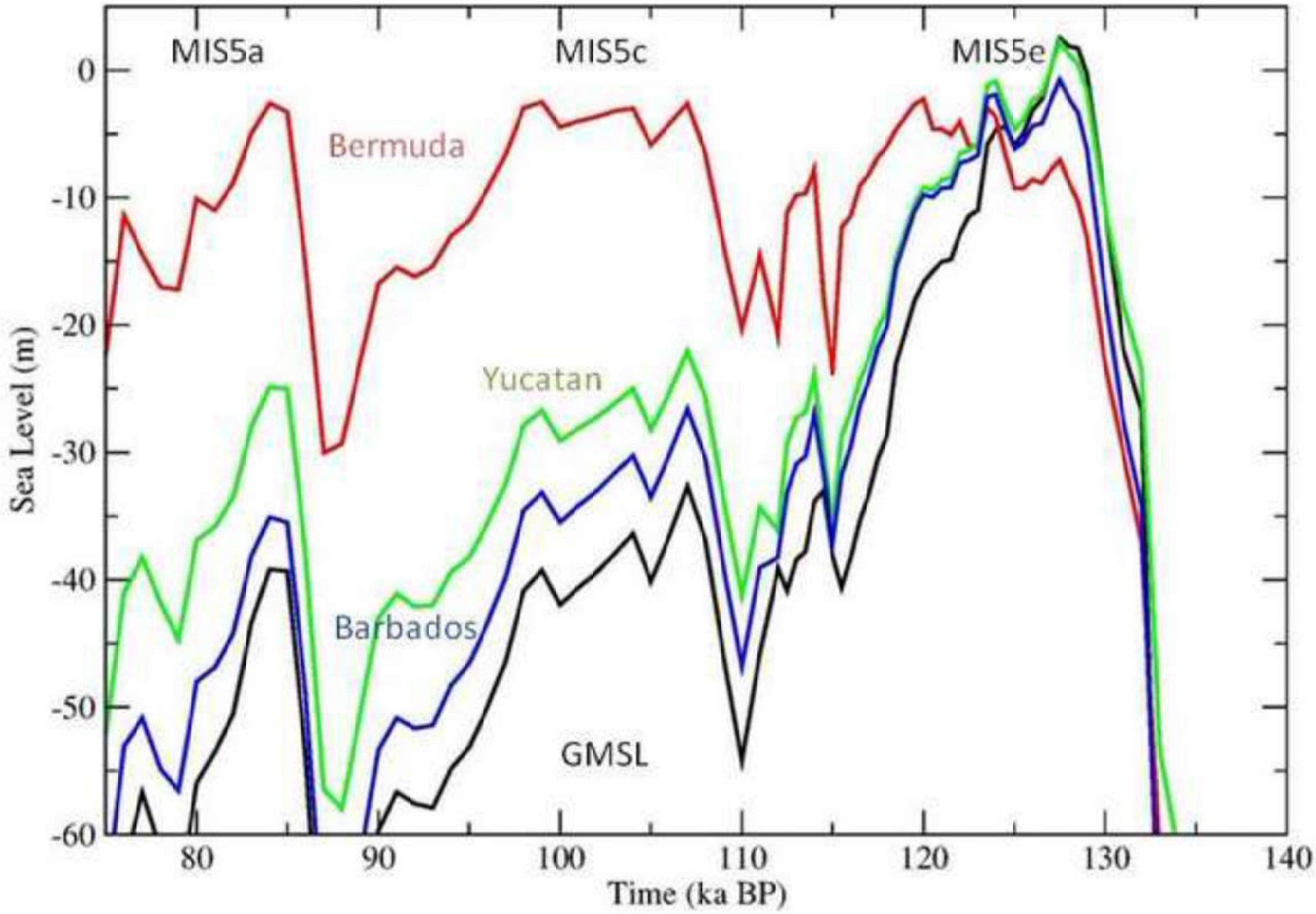

Figure 9

Table 1

Click here to download Table: Table1w.docx

Discontinuity ID	Age ka BP (2σ uncertainties)	MIS	duration ±2σ (ka)	Petrographic change	New generation with competitive crystal growth
Discontinuity in M777	159-83.5	5e-d-c-b	79.5	biogenic incrustation	No observation
Discontinuities in QB					
D1	137.0±4.9 to 114.7±4.5	5e	22.4±7.0	DCC to WPC large and fragile crystals	yes, continously
D2	105.9±6.4 to 92.0±3.1	5c	13.8±7.1	WPC to generally denser calcite	No
D3	84.3±1.5 to 82.0 ±1.1	5a	2.4±1.8	Set of more porous layers, appearing whistish in between two denser calcite deposition episods	No
D4	79.9±0.9 to 75.0±0.8	5a'	4.9±1.2	Set of more porous layers, appearing whistish in between two denser calcite deposition episods	At some places
D5				DCC to WPC with an increasing occurrence of clayey layer	No

Table S1

Click here to download Table: Table S1word.docx

Table S1:U-series data and location of discontinuities for sample QB. Discontinuities are marked by a red shade. 95% error bars are provided. The following recently updated half-lives were used to compute the results: 245,620 ± 260 yrs for ^{234}U and 75,584 ± 110 yrs for ^{230}Th (Cheng et al., 2013). Uncorrected ages are given relative to their date of analyse while the corrected ages BP are provided relatively to 1950 and corrected for initial ^{230}Th using the bulk earth value of $^{230}Th/^{232}Th$ detrital activity ratio of 0.8±0.4 assuming a $^{232}Th/^{238}U$ mass ratio of 3.8 (Wedepohl, 1995). 234U/238U initial ratios are corrected for initial Th.

Sample QB subsample's ID	MIS	cm/ref on the ref axis	^{238}U ppb	$^{232}Th/^{238}U$ activity ratio	±	$^{230}Th/^{238}U$ activity ratio	±	$^{234}U/^{238}U$ activity ratio	±	$^{232}Th/^{230}Th$ activity ratio	±	Uncorrected age years	err+	err-	$^{234}U/^{238}U_{initial}$ activity ratio	err+	err-	Corrected age yrs BP	err+	err-
B1BiA	MIS6	*-0.2*	199	3.328E-04	1.599E-05	0.7519	0.0046	1.0292	0.0051	4.43E-04	2.14E-05	141593	2222	2209	1.0434	0.0076	0.0074	**141503**	**2222**	**2216**
B1Bi7	MIS6	*-0.1*	230	1.537E-04	9.793E-04	0.7461	0.0035	1.0243	0.0043	2.06E-04	1.31E-03	140486	1723	1684	1.0360	0.0063	0.0065	**140409**	**1734**	**1681**
B1Cii_1	MIS6	0	284	1.994E-04	9.428E-06	0.6492	0.0034	1.0122	0.0051	3.07E-04	1.45E-05	111468	1353	1340	1.0434	0.0073	0.0075	**139479**	**2031**	**1995**
D1	MI5e	0.3																		
B1Cii_2	MIS5d	0.5	224	3.618E-04	1.404E-05	0.7469	0.0043	1.0293	0.0051	4.84E-04	1.88E-05	139571	2035	1992	1.0167	0.0067	0.0070	**111389**	**1357**	**1342**
B3_1	MIS5d	0.6	342	5.191E-04	9.013E-06	0.6422	0.0032	1.0095	0.0045	8.08E-04	1.41E-05	109991	1167	1213	1.0130	0.0061	0.0062	**109884**	**1178**	**1208**
B1BiB	MIS5d	0.65	280	5.264E-04	1.279E-05	0.6557	0.0039	1.0083	0.0048	8.03E-04	1.98E-05	114352	1549	1477	1.0114	0.0064	0.0069	**114245**	**1551**	**1477**
D2	MIS5c	0.9																		
B1Cii5	MIS5b	1.1	381	8.377E-08	1.043E-03	0.5695	0.0033	1.0007	0.0044	3.14E-08	1.84E-03	91782	952	933	1.0009	0.0056	0.0059	**91718**	**947**	**924**
B1Bi6	MIS5b	1.25	375	1.351E-04	6.046E-04	0.5607	0.0034	1.0039	0.0040	2.41E-04	1.08E-03	89049	965	932	1.0051	0.0051	0.0052	**88973**	**959**	**929**
B1BiC	MIS5b	1.85	360	2.273E-04	1.230E-05	0.5523	0.0030	1.0064	0.0047	4.12E-04	2.24E-05	86682	930	892	1.0081	0.0061	0.0061	**86601**	**929**	**894**
B1Bi8	MIS5b	2.15	512	8.041E-05	3.251E-04	0.5465	0.0021	1.0039	0.0035	1.47E-04	5.98E-04	85660	587	537	1.0049	0.0044	0.0046	**85589**	**590**	**535**
D3	i5a(early	2.4																		
B1Bi5	MIS5a	2.65	318	1.253E-04	7.333E-04	0.5365	0.0034	1.0169	0.0042	2.34E-04	1.36E-03	81536	854	830	1.0212	0.0053	0.0053	**81462**	**849**	**816**
B1Cii6	MIS5a	3.65	330	8.606E-05	4.930E-04	0.5313	0.0022	1.0176	0.0038	1.62E-04	9.21E-04	80303	557	579	1.0220	0.0046	0.0049	**80231**	**558**	**580**
D4	S5a(late I	3.8																		
B1Cii7	MIS5a	3.9	236	4.244E-04	8.715E-04	0.5112	0.0036	1.0242	0.0056	8.30E-04	1.70E-03	75120	899	897	1.0298	0.0070	0.0068	**75070**	**897**	**895**
B1Bi4	MIS5a	4.2	370	2.171E-04	6.347E-04	0.5069	0.0029	1.0252	0.0042	4.28E-04	1.26E-03	74117	696	679	1.0310	0.0051	0.0051	**74034**	**689**	**672**
B1Cii4	MIS5a	4.75	241	4.564E-04	9.871E-04	0.5096	0.0036	1.0397	0.0049	8.96E-04	1.94E-03	73082	796	799	1.0487	0.0060	0.0059	**72980**	**787**	**772**
B2B	MIS5a	5.15	153	1.652E-03	5.656E-05	0.5118	0.0061	1.0434	0.0081	3.23E-03	1.13E-04	73130	1416	1404	1.0532	0.0098	0.0098	**72930**	**1412**	**1412**

Table S2

Click here to download Table: Table S2word.docx

Table S2: U-Th data, location and elevation of the stump of the other samples in this study. 95% error bars are provided. The same half-lives and values for detrital correction than in table S1 were used to compute the results. $^{234}U/^{238}U$ initial ratios are corrected for initial Th. For M777, Crystal Cave, M1 is actually the subsample collected the closer to the hiatus, just under it. Some dissolution-reprecipitation is suspected for this sub-sample as its U concentration is about 80% less than the concentration of the others. M3 was thus collected a little bit further and lead to a more realistic age.

ID	Altitude masl	^{238}U ppb	$^{232}Th/^{238}U$ activity ratio	±	$^{230}Th/^{238}U$ activity ratio	±	$^{234}U/^{238}U$ activity ratio	±	$^{232}Th/^{230}Th$ activity ratio	±	Uncorrected age years	err+	err-	$^{234}U/^{238}U_{initial}$ activity ratio	err+	err-	**Corrected age years BP**	**err+**	**err-**
Admiral cave																			
Admiral stal	10																		
Ext slice																			
Ad-18		73	4.9618E-03	5.1799E-05	0.38700	0.00687	1.08058	0.00569	7.800E+01	1.544E+00	48059	1136	1058	1.09192	0.00602	0.00693	**47479.75**	**1240**	**1192**
discontinuity																			
Ad-17		82	1.5672E-03	6.2676E-05	0.46089	0.00945	1.07307	0.00713	2.941E+02	1.310E+01	60736	1713	1691	1.08682	0.00875	0.00794	**60503.78**	**1730**	**1698**
Ad-16		96	9.8621E-04	1.3260E-05	0.45997	0.00373	1.07064	0.00458	4.664E+02	6.900E+00	60782	673	673	1.08370	0.00540	0.00543	**60611.79**	**678.9**	**662.5**
discontinuity																			
AD5EXT		59	2.8693E-02	9.0661E-04	0.55243	0.02236	1.05631	0.03332	1.925E+01	5.536E-01	80162	6132	5592	1.07096	0.04062	0.04086	**77743.63**	**6186**	**5687**
disc																			
Ad-19		116	4.8024E-03	5.1532E-05	0.53324	0.00832	1.05541	0.00615	1.110E+02	2.011E+00	76183	1834	1721	1.06849	0.00777	0.00727	**75606.51**	**1906**	**1798**
Ad-15		131	7.9483E-04	2.7518E-05	0.52894	0.00718	1.05201	0.00532	6.655E+02	2.430E+01	75654	1614	1503	1.06440	0.00661	0.00638	**75503.09**	**1605**	**1513**
discontinuity																			
Ad-9		183	3.4810E-04	1.2645E-05	0.58008	0.00328	1.05968	0.00509	6.001E-04	2.204E-05	85618	854	853	1.07603	0.00623	0.00653	**85527**	**857**	**851**
discontinuity																			
Ad-8		124	1.3655E-03	2.1549E-05	0.82449	0.00531	1.04852	0.00610	1.656E-03	2.638E-05	164645	3126	3036	1.07724	0.00909	0.00934	**164471**	**3113**	**3019**
Ad-7		152	4.0812E-03	2.9495E-05	0.81547	0.00537	1.04278	0.00590	5.005E-03	4.085E-05	162949	3032	2929	1.06772	0.00875	0.00921	**162549**	**3049**	**2918**
discontinuity																			
Ad-6		245	3.9419E-04	8.5298E-06	0.85839	0.00467	1.04259	0.00437	4.592E-04	1.022E-05	184470	3081	3016	1.07177	0.00692	0.00720	**184375**	**3078**	**3008**
Ad-10		398	4.2358E-04	8.0896E-06	0.86782	0.00379	1.03914	0.00431	4.881E-04	9.412E-06	191939	2792	2838	1.06716	0.00669	0.00729	**191842**	**2792**	**2836**
bicolorblock																			
AD1		778	1.1227E-04	5.6443E-06	0.88077	0.00389	1.03328	0.00360	1.275E-04	6.431E-06	203928	3043	3075	1.05906	0.00601	0.00618	**203856**	**3046**	**3074**
discontinuity																			
AD2		605	2.5501E-04	1.1304E-05	0.86023	0.00321	1.03858	0.00389	2.964E-04	1.329E-05	187833	2460	2339	1.06548	0.00623	0.00642	**187750**	**2465**	**2328**
Heart piece																			
AD3 COEUR		521	5.4786E-05	1.1492E-05	0.89547	0.00370	1.03521	0.00400	6.118E-05	1.282E-05	212730	3431	3389	1.06397	0.00696	0.00689	**212664**	**3429**	**3390**
Newblock																			
Ad14		422	2.7303E-05	3.0728E-04	0.89234	0.00305	1.03349	0.00378	3.060E-05	3.435E-04	211784	2945	2724	1.06076	0.00678	0.00637	**211718**	**2939**	**2726**
discontinuity																			
Ad11		879	7.5339E-05	3.2439E-04	0.85384	0.00385	1.03171	0.00364	8.824E-05	3.784E-04	188144	2687	2627	1.05379	0.00612	0.00585	**188074**	**2690**	**2627**
Ad13		562	2.5340E-05	1.4612E-04	0.88643	0.00267	1.03427	0.00349	2.859E-05	1.649E-04	207040	2303	2418	1.06135	0.00597	0.00593	**206974**	**2304**	**2415**
discontinuity																			
Ad12		436	4.3164E-04	5.5116E-04	0.89868	0.00443	1.03389	0.00403	4.803E-04	6.148E-04	216118	4049	3884	1.06212	0.00689	0.00716	**216018**	**4042**	**3875**
Stump																			
Adstump1		694	6.2114E-05	1.7133E-04	0.86452	0.00332	1.03910	0.00368	7.185E-05	1.986E-04	190027	2454	2249	1.06682	0.00594	0.00610	**189958**	**2457**	**2253**
Adstump2		347	3.5335E-04	2.4100E-04	0.87728	0.00385	1.03535	0.00374	4.028E-04	2.723E-04	200200	3052	2915	1.06220	0.00641	0.00611	**200108**	**3050**	**2901**
Camp S. David Flowstones B & C	2																		
FB2-1		90	1.0093E-02	7.6122E-05	0.78533	0.00713	1.05908	0.00767	1.285E-02	1.124E-04	144407	3335	3288	1.08858	0.01114	0.01097	**143532**	**3372**	**3296**
FB1-2		118	5.0913E-04	1.7808E-05	0.84675	0.00780	1.05305	0.00599	6.012E-04	2.056E-05	173147	4453	3795	1.08632	0.00951	0.00927	**173043**	**4465**	**3798**
FB1		174	8.7395E-03	9.8204E-05	0.88130	0.01791	1.05176	0.00911	9.900E-03	2.000E-04	192200	11551	10419	1.08923	0.01488	0.01479	**191437**	**11573**	**10419**
FlowstoneC		160	1.3799E-04	8.0330E-04	0.82654	0.00439	1.06610	0.00496	1.670E-04	9.681E-04	158326	2350	2309	1.10341	0.00743	0.00729	**158252**	**2342**	**2293**

Walsingham cavern sample W1	-1																		
W1-1G1		65	3.2486E-03	7.0004E-05	0.05050	0.01120	1.00412	0.01301	6.432E-02	1.439E-02	5637	1309	1277	1.00442	0.01356	0.01282	**5289**	**1315**	**1300**
W1-3G1		33	6.0314E-03	1.6016E-04	0.08640	0.01478	1.02190	0.02061	6.980E-02	1.203E-02	9635	1777	1734	1.02300	0.02139	0.02092	**9055**	**1773**	**1749**
Crystal cave																			
sample77010	-13.7																		
drap0131		131	3.3886E-04	2.1945E-05	0.30459	0.00288	1.03733	0.00497	1.113E-03	7.292E-05	37819	466	437	1.04154	0.00551	0.00549	**37726**	**463**	**440**
drap0132		105	2.9771E-04	3.5582E-05	0.33370	0.00240	1.04456	0.00442	8.921E-04	1.076E-04	41851	403	372	1.05001	0.00492	0.00497	**41762**	**403**	**373**
sample770302-1	-11																		
lgriz0211		70	6.3320E-05	2.9931E-05	0.38453	0.00395	1.03127	0.00560	1.647E-04	7.817E-05	50751	730	702	1.03606	0.00650	0.00637	**50682**	**728**	**702**
lgriz0212		23	2.6954E-02	3.5207E-04	0.39613	0.01033	1.03694	0.01352	6.804E-02	1.648E-03	52331	1961	1854	1.04260	0.01520	0.01562	**49984**	**2300**	**2250**
sample770302-5	-13.5																		
crep0251		50	3.0294E-04	3.4615E-05	0.102075	0.002747	1.075033	0.00579	2.968E-03	3.489E-04	10868.2572	320.1	304.5	1.077325	0.0061	0.0059	**10779.614**	**318.4**	**303.5**
crep0252		33	7.8571E-04	5.5408E-05	0.089401	0.004228	1.065778	0.00868	8.789E-03	7.462E-04	9546.42355	468.5	477.3	1.067531	0.009	0.0088	**9418.0593**	**472.9**	**474.6**
Squeeze cave																			
sample S1	1.4																		
S1_1		25	1.0105E-02	8.0675E-04	0.118332	0.122548	1.056416	0.06944	8.540E-02	8.754E-02	14031.2808	16455	12560	1.095789	1.0583	0.0736	**13596.277**	**18852**	**12091**
S1-3		49	7.4322E-04	6.8346E-05	0.095369	0.007584	1.064348	0.01507	7.793E-03	9.366E-04	10218.9695	850.3	858.3	1.066569	0.0153	0.0157	**10095.441**	**866.7**	**854.3**
S1-4		57	3.9594E-03	8.1609E-05	0.053377	0.008046	1.07037	0.01475	7.418E-02	1.114E-02	5584.69343	883.3	846.6	1.071746	0.0149	0.0149	**5199.1443**	**908.3**	**873**
sampleS2	1.9																		
S2_1		49	6.3525E-04	2.3989E-04	0.089648	0.070498	1.068654	0.03862	7.086E-03	6.151E-03	9600.54812	8363	7406	1.071032	0.0393	0.0399	**9490.1041**	**8368**	**7400**
S2_2		51	7.0200E-03	3.2369E-04	0.015386	0.04745	1.093149	0.0387	4.562E-01	1.402E+00	4408.55925	1159	1173	1.107234	0.0091	0.0072	**3789.0758**	**1234**	**1227**
S2-3		65	9.5658E-04	6.2232E-05	0.09112	0.006155	1.085346	0.015	1.050E-02	9.583E-04	9559.56101	679.5	681.7	1.087957	0.0155	0.0153	**9419.644**	**676.8**	**680.8**
Sample S3	2.2																		
S3_2		9	1.0981E-03	1.4846E-04	0.044926	0.010132	1.077503	0.02336	2.444E-02	6.416E-03	4642.04285	1063	1087	1.078918	0.0232	0.024	**4490.8049**	**1070**	**1083**
S3_1		42	1.1326E-02	5.9886E-04	0.143245	0.02468	1.074575	0.04885	7.907E-02	1.355E-02	15573.727	3028	2915	1.077265	0.0513	0.0503	**14602.815**	**2958**	**2926**
Belle	8.5																		
Belle-bell1		70	9.8005E-02	5.7673E-03	0.268862	0.01538	1.068757	0.0088	3.645E-01	2.953E-02	31513.5599	2069	2117	1.073478	0.0096	0.0092	**23220.819**	**4704**	**4794**
Belle-bell2		72	8.6683E-02	3.3168E-03	0.258131	0.010346	1.068661	0.0061	3.358E-01	1.854E-02	30069.1528	1413	1383	1.07304	0.0066	0.0065	**22753.515**	**3995**	**4066**
Belle-bell3		39	4.1291E-03	9.6489E-03	0.398023	0.014177	1.079028	0.01409	1.037E-02	2.436E-02	49922.8732	2388	2244	1.090858	0.016	0.0161	**49563.745**	**2125**	**1988**

Wilkinson Quarry cave (others)																				
Sample C	0.4																			
C3A		315	3.3817E-04	1.4568E-05	0.163225	0.001059	1.054959	0.00392	2.072E-03	9.061E-05	18306.8557	139.7	135.6	1.057726	0.004	0.0043	**18216.77**	**139.5**	**134.9**
C4C		189	3.1541E-04	2.1116E-05	0.133348	0.002216	1.052817	0.00567	9.099E-03	2.288E-04	14755.1892	276.2	263.5	1.055004	0.0059	0.0059	**14667.079**	**274.4**	**264.5**
C4D		153	6.3155E-04	3.2178E-05	0.12924	0.003072	1.046834	0.0076	1.630E-02	1.671E-02	14353.1114	388.7	362.1	1.048632	0.0078	0.008	**14238.369**	**384.7**	**366.6**
C4B		149	1.1801E-03	2.4721E-05	0.129698	0.001879	1.047906	0.00574	9.099E-03	2.288E-04	14390.787	235.6	231.6	1.0499	0.0061	0.0058	**14231.571**	**244.2**	**236.5**
C4A		223	3.5293E-04	2.7285E-05	0.049143	0.001461	1.066417	0.00459	7.182E-03	5.949E-04	5142.50459	158.7	156.2	1.067283	0.0046	0.0047	**5051.6799**	**158.2**	**157.7**
Sample A	1.4																			
A1B		219	4.2394E-03	4.3252E-03	0.260072	0.027509	1.070728	0.00544	1.630E-02	1.671E-02	30251.0882	3785	3581	1.076906	0.0063	0.0057	**29843.934**	**3415**	**3240**
A1A		323	1.7729E-04	1.6623E-05	0.190825	0.001322	1.082067	0.00416	9.291E-04	8.807E-05	21110.7305	176.5	159.2	1.086915	0.0044	0.0044	**21034.449**	**177.5**	**160**
A3A		225	4.2444E-04	2.3992E-05	0.181337	0.002038	1.070982	0.00567	2.341E-03	1.331E-04	20186.6604	272.5	267.7	1.075074	0.006	0.0059	**20090.255**	**275.6**	**266.3**
Sample E	-0.2																			
E1A		193	9.6981E-04	2.2280E-05	0.093735	0.001426	1.046537	0.00561	1.035E-02	2.795E-04	10224.8748	169.3	171.2	1.047852	0.0059	0.0056	**10081.809**	**179.2**	**177.4**
E1B		179	1.9175E-03	2.9301E-05	0.076204	0.001545	1.038568	0.00432	2.516E-02	6.298E-04	8304.71755	171.6	180.6	1.039411	0.0043	0.0045	**8081.9554**	**195.1**	**202.4**
Sample D	0.3																			
D1A		140	7.5797E-04	4.9713E-05	0.256183	0.0035	1.088333	0.00533	2.959E-03	1.985E-04	29158.6836	467.2	469.8	1.09576	0.0057	0.0058	**29036.076**	**463.1**	**470.1**
D1B		179	1.5792E-03	1.8060E-03	0.102924	0.014055	1.072974	0.0052	1.534E-02	1.762E-02	10984.7845	1593	1568	1.075173	0.0054	0.0053	**10795.117**	**1473**	**1459**
Sample QB tip																				
B5C	0.5	206	6.2202E-04	2.2210E-05	0.364185	0.003224	1.038646	0.00614	1.708E-03	6.111E-05	46933.121	582.2	600.4	1.044085	0.007	0.0069	**46819.067**	**583.4**	**602.5**
B5A	0.5	218	1.0597E-03	3.5644E-04	0.451325	0.04143	1.036694	0.02835	2.348E-03	8.081E-04	62122.0247	7870	7537	1.043962	0.0335	0.0335	**61971.333**	**7882**	**7510**

Supplementary material for online publication only

Click here to download Supplementary material for online publication only: Supp mat_15072016pm-last.docx